UNIVERSITY OF THE PHILIPPINES

Bachelor of Science in Physics

Mark Ivan Gabo Ugalino

Density perturbation induced by relativistic bodies in slightly-eccentric orbits

Thesis Adviser:

Michael Francis Ian Vega II, PhD

National Institute of Physics

University of the Philippines Diliman

In Partial Fulfillment of the Requirements
for the Degree of
Bachelor of Science in Physics

Date of Submission:
June 2018

Thesis Classification:
P

National Institute of Physics
College of Science
University of the Philippines
Diliman, Quezon City

ENDORSEMENT

This is to certify that this thesis entitled **Density perturbation induced by relativistic bodies in slightly-eccentric orbits**, prepared and submitted by **Mark Ivan Gabo Ugalino** to fulfill part of the requirements for the degree of Bachelor of Science in Physics was successfully defended and approved on 07 May 2018.

MICHAEL FRANCIS IAN G VEGA II,
Ph.D.
Thesis Adviser

The National Institute of Physics endorses acceptance of this thesis as partial fulfillment of the requirements for the degree of Bachelor of Science in Physics.

ROLAND V SARMAGO, Ph.D.
Director
National Institute of Physics

The thesis is hereby officially accepted as partial fulfillment of the requirements for the degree of Bachelor of Science in Physics.

PERRY S ONG, Ph.D.
Dean
College of Science

In loving memory of

Mario Gaspar Ugalino Sr.
(May 5, 1964- August 19,2015)

who had perfected the art of self-giving

Acknowledgments

ABSTRACT

DENSITY PERTURBATION INDUCED BY RELATIVISTIC BODIES IN SLIGHTLY-ECCENTRIC ORBITS

Mark Ivan Gabo Ugalino
University of the Philippines (2018)

Adviser:
Michael Francis Ian G Vega II, Ph.D.

We consider a massive perturber moving along slightly-eccentric orbits through a collisional fluid in flat spacetime. We evaluate, via a frequency-domain calculation, the density perturbations induced by this massive perturber and reproduce the characteristic spiral wave structure previously computed for circular orbits with time-domain methods. This work serves as a precursor to a full calculation of the relativistic dynamical friction (DF) experienced by a perturber moving along a slightly-eccentric orbit. Our slightly-eccentric analysis is restricted by three conditions: (a) the perturbations are kept in linear order, (b) the weak-field region of the perturbed Schwarzschild spacetime is approximated as a perturbed Minkowski background, and (c) the fluid and the moving particle exist perpetually, ie. the perturbation was turned on long before the system was observed.

PACS: 95.30.Lz - Hydrodynamics, 95.30.Sf - Relativity and gravitation, 95.10.Eg - Orbit determination and improvement

Table of Contents

List of Figures

List of Symbols

$a, b, c, ...$	Spatial components (*if used as an index*)
$\alpha, \beta, \gamma, ...$	Spatial and temporal components (*if used as an index*)
δ_{ij}	Kronecker delta
∇^2	Laplacian ($\nabla \cdot \nabla$)
∂_i	Gradient (*in arbitrary coordinates*)
$\Box$	D'Lambertian, ($\Box = \eta^{\mu\nu}\partial_\mu\partial_\nu$)

Chapter 2

$\phi,\ \psi$	Metric perturbation functions
ω_i	Three-vector metric component
$\omega^{\parallel}$	Divergence-free (*longitudinal*) component of ω_i
$\omega_i^{\perp}$	Curl-free (*transverse*) component of ω_i
χ_{ij}	Four-tensor metric component
$\chi^{\parallel}$	Trace part of χ_{ij}
$\chi_j^{\perp}$	Curl-free part of χ_{ij}
$\chi_{ij}^{\perp}$	Divergence-free part of χ_{ij}
$\tilde{g}_{\mu\nu}$	Perturbed metric tensor
dx^μ	One-form gradient of x^μ
x^μ	arbitrary scalar coordinate field
$T_{\mu\nu}$	Stress-energy tensor
T_{tt}	Energy-density component of $T_{\mu\nu}$
T	Spatial trace of $T_{\mu\nu}$, ($T = \delta^{ij}T_{ij}$)
$\varepsilon_1,\ \varepsilon_2$	Perturbation parameters
$\mathcal{L}$	Characteristic size of an enveloping medium
λ_J	Generalized Jeans length
M	Mass of a moving perturber

r_{min}	cutoff radius, (*to avoid divergent expansion parameter* ε_2)
$T_{\mu\nu}^{\text{pert}}$	Stress-energy due to the presence of the perturber
$T_{\mu\nu}^{\text{fluid}}$	Stress-energy due to the presence of the fluid
ρ	energy density
p	pressure
$\tilde{\rho}$	perturbed energy density
$\tilde{p}$	perturbed pressure
$\tilde{u}_\mu$	perturbed four-velocity
$\tilde{n}$	perturbed number density
$\tilde{a}^\mu$	perturbed four-acceleration
$\frac{\delta n}{n}$	dimensionless density perturbation
c_s	speed of sound in a fluid
γ	Lorentz boost factor
Ω	Angular velocity
M_{BH}	Mass of a black hole
R_g	Gravitational radius
ϕ^{fluid}, ψ^{fluid}	Metric perturbations due to the fluid
$\delta g_{\mu\nu}^{\text{fluid}}$	
ϕ^{pert}, ψ^{pert}	Metric perturbations due to the perturber
$\delta g_{\mu\nu}^{\text{pert}}$	
R	orbital radius
$\mathcal{D}(\mathbf{x}, t)$	Weight function (Kim and Kim 2007)
$\mathcal{M}$	Mach number of a moving object in a fluid, ($\mathcal{M} = \frac{v}{c_s}$)
$\hat{x}^i$	Coordinates scaled to the orbital radius, $\hat{x} = \frac{x}{R}$

Chapter 3

$R(t)$	Time parameterized radial orbit constraint
$\Phi(t)$	Time parameterized azimuthal orbit constraint
Ω_o	Unperturbed angular frequency of the orbit
r_o	Unperturbed radius of the orbit
Ω_ϕ	Azimuthal fundamental frequency of the orbit
Ω_r	Radial fundamental frequency of the orbit
δR	Perturbation parameter

ω_m^o	Main frequency
$\omega_m^{\pm}$	Sideband frequencies
ρ_{lm}	Spherically decomposed source
v	velocity of the perturber
ω	angular frequency of the orbit (*in general*)
$\Theta(\cdot)$	Heaviside distribution
$\Psi_+,\ \Psi_-$	Solutions inside and outside the orbital radius
$\Psi^o_{lm,\ \pm}$	Solution due to the main frequency
$\chi^{\pm}_{lm,\ \pm}$	Solutions due to the sideband frequencies
Ω_{pr}	Precession frequency, ($\Omega_{pr} = \Omega_o - \Omega_r$)
$\mathcal{W}$	Weight function
$\eta^{\mu\nu}$	unperturbed Minkowski metric

Chapter 1

Introduction

1.1 Invitation

The interaction between a massive moving body with its gravitationally induced wake gives rise to a momentum loss known as *dynamical friction* (DF). The analytic theory of DF for a collisionless system was first formulated by Subrahmanyan Chandrasekhar in his seminal paper on the subject [1], the result of which has since been verified in observed astronomical systems, and applied to numerical simulations over the past several years. Its consequences have been instrumental in theoretically describing the sinking of orbiting satellites towards their parent galaxy [2, 3, 4], planet migration [5], the growth of planetisimals [6], and the dynamical evolution of star clusters near the galactic center [7, 8, 9], among many others. It was computed in the Post-Newtonian approximation by Lee [10] for the same uniform and isotropic system, and was later extended to a fully relativistic treatment by Petrich et al [11] for a moving Schwarzschild black hole of mass M.

Although less well-known, DF also operates in a gaseous environment (i.e. collisional systems). For bodies travelling in supersonic speeds, the drag force approaches the same expression for the collisionless case. However, it was found that the drag is absent in the subsonic case because of the upwind-downwind symmetry, in both relativistic and non-relativistic formulations [11, 12]. It was not until the finite-time analysis of Ostriker [13] for the straight-line case, and Kim & Kim [14] for circular orbits, that dynamical friction was characterized for both subsonic and supersonic motion in collisional systems.

In most cases, a Newtonian treatment is enough to describe the behavior of an astronomical system. However, in the limit where orbital velocities reach the speed of light, such as the case for extreme-mass ratio inspirals (EMRIs) [15], a relativistic extension is necessary to accurately describe the evolution of the system. Enrico Barausse laid the framework for the relativistic extension of DF in collisional systems by using tools from general relativity [16], while closely following the methods used by Ostriker, and Kim & Kim, that is by analyzing DF effects for straight-line motion and circular orbits on flat spacetime.

In this introductory chapter, we set the stage with a survey of the past literature. We revisit the DF theory of Chandrasekhar closely following the discussion by Binney and Tremaine [17]. An outline of the extension to the collisional case is presented through a discussion of Ostriker and Kim & Kim's findings and its implications in both subsonic and supersonic regimes. This culminates in a review of what extreme-mass ratio inspirals are and the relevance of DF in its dynamics. The organization of this manuscript is presented by the end of this chapter.

1.2 Chandrasekhar's dynamical friction and extensions thereof

1.2.1 Collisionless systems: Chandrasekhar (1943)

A massive perturber, such as a star, moving through a homogeneous field of surrounding stellar objects may experience velocity fluctuations due to the gravitational pull of nearby field objects. Therefore, we can think of its motion as that of a body that experiences velocity increments due to *random* directions. This would mean that the motion of the perturber would satisfy the diffusion equation,

$$\frac{\partial W}{\partial t} = q\nabla^2_{\mathbf{u}}W \tag{1.1}$$

where q is the coefficient of diffusion, whose solution W deviates from a Maxwellian distribution for large periods of time. Thus, this prescription implies that the system is *non-conservative*, which does not agree with our physical considerations, that is our system is *adiabatic*. Chandrasekhar argued that the diffusion equation must have a missing term that is akin to that of the formalism applied by Uhlenbeck and Ornstein [18] for Brownian motion. Thus, he added a decelerative component such that for a

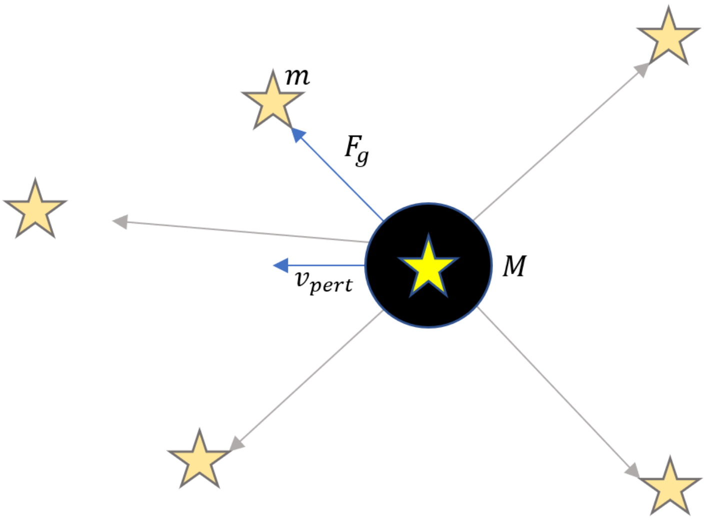

Figure 1.1: Gravitational interaction of a moving perturber of mass M to gravitating field objects of mass m. The moving perturber experiences *random* velocity fluctuations due to the gravitational pull of each field object that is distributed over space.

short period of time Δt, the moving body experiences velocity increments Δu,

$$\Delta u = \delta u - \eta u \Delta t$$

where δu is governed by the solution of Equation [1.1], and the latter term is the acceleration opposite to the motion of the perturber and proportional to the magnitude of its velocity $\mathbf{u}$, and a coefficient of friction η. Arguing that the stochastic process that the perturber undergoes must tend to a Maxwellian distribution for large times, due to energy conservation, therefore implies that any kind of perturber must experience a gravitational drag, or *dynamical friction* [1].

One can proceed in solving for the dynamical friction effects on a perturber of mass M moving through a homogeneous field of objects of individual mass m, by treating each successive encounter as a two-body approximation, and add up all the effects with all field objects that can be influenced by the gravitational potential of the moving perturber. In other words, one can imagine this problem as a two-body scattering system as shown below,

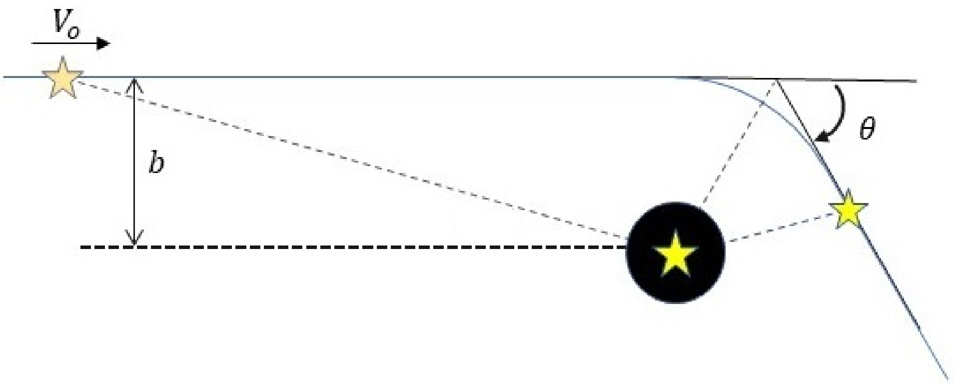

Figure 1.2: An encounter between a massive object of mass M, and a field object of mass m represented by the hyperbolic motion of a reduced particle of mass $M + m$ moving with speed V_o from infinity, with impact parameter b.

where θ is the angle of deflection of the reduced particle from the original trajectory; and, b is the length of the component of the separation vector between a field object from infinity and a massive moving object, perpendicular to the initial velocity vector of the field object, which is also known as the *impact parameter*.

The motion of the reduced particle in this approximation would then have induced velocity increments opposite the trajectory of the perturber, which has transverse and longitudinal components of the form [17],

$$|\Delta v_{M\perp}| = \frac{2mbV_o^3}{G(M+m)^2}\left[1 + \frac{b^2V_o^4}{G^2(M+m)^2}\right]^{-1} \tag{1.2}$$

$$|\Delta v_{M\parallel}| = \frac{2mV_o}{M+m}\left[1 + \frac{b^2V_o^4}{G^2(M+m)^2}\right]^{-1} \tag{1.3}$$

where V_o is the velocity of the reduced particle. We imagine that this massive perturber is moving amongst an infinite homogeneous distribution of stellar field objects, such that we consider the effect of each stellar encounter on the perturber. By effectively ignoring the potential due to the homogeneous field of stars by invoking Jeans' swindle [19], one can consider that only the perturber would have a gravitational influence on the system. By invoking the planar symmetry of the system, the sum over all contributions by each field object will have no transverse component, while the longitudinal component adds up to a non-zero resultant given by an integration of $\Delta v_{M\parallel}$ over all possible values of b [17],

$$\left.\frac{\mathrm{d}v_M}{\mathrm{d}t}\right|_{v_M} = V_o f(v_m)\mathrm{d}^3 v_m \int_0^{b_{max}} |\Delta v_{M\parallel}|\; 2\pi b\; db.$$

which implies that it is as if there were an effective clump of matter behind the trajectory of the moving perturber, inducing a gravitational drag that is DF. Evaluating the integral over b, that is considering all possible configurations of stellar field objects, gives us

$$\left.\frac{\mathrm{d}v_M}{\mathrm{d}t}\right|_{v_M} = 2\pi \ln(1+\Lambda^2) G^2 m(M+m) f(\mathbf{v}_m) d^3\mathbf{v}_m \frac{\mathbf{v}_m - \mathbf{v}_M}{|\mathbf{v}_m - \mathbf{v}_M|^3} \tag{1.4}$$

where

$$\Lambda \equiv \frac{b_{max} V_o^2}{G(M+m)}$$

While applying Coulomb's algorithm, $\frac{1}{2}\ln(1+\Lambda^2) \approx \ln\Lambda$, and proceeding with the analysis in the approximation that $\ln\Lambda$ is constant, integrating Equation (1.4) while assuming that the distribution of velocities is isotropic, yields Chandrasekhar's formula for dynamical friction,

$$\frac{\mathrm{d}\mathbf{v}_M}{\mathrm{d}t} = -16\pi^2 \ln\Lambda G^2 m(M+m) \int_0^{v_M} f(v_m) v_m^2 dv_m \frac{\mathbf{v}_M}{v_M^3}. \tag{1.5}$$

This implies that to a certain level of accuracy the only field objects moving slower than the perturber contribute to the change in velocity [1].

1.2.2 Collisional systems: Ostriker (1999) and Kim and Kim (2007)

Collisionless and collisional systems in astrophysics

We have previously discussed Chandrasekhar's formulation of dynamical friction for collisionless systems, which is particularly useful in describing the dynamics of stellar objects in the galactic scale. This treatment works because in this scale, stellar populations, such as stellar clusters, weakly interact because gravity is a weak long-range force. One can also observe that the collision cross-section between stellar clusters are usually minute even for bulk configurations since separation distances between stars are usually large, which implies that there is not enough time for any interaction to occur. However, typical galaxies also have a gaseous component (i.e. collisional) which motivates an extension of DF as a gaseous drag force. In this case, we account for the interaction of gas particles in terms of *collisions* which affect the evolution of the density function $f(\mathbf{r}, \mathbf{p}, t)$ that tells us the probability for a particle in a fluid to have a certain position $\mathbf{r}$ and momentum $\mathbf{p}$ in phase space. In a non-equilibrium state, this density function evolves according to the *Boltzmann* equation given by [20],

$$\frac{\partial f}{\partial t} + \frac{\mathbf{p}}{m} \cdot \nabla f + \mathbf{F} \cdot \frac{\partial f}{\partial \mathbf{p}} = \left(\frac{\partial f}{\partial t}\right)_{collision}$$

where for cases when the collision term on the right hand side is zero, as in collisionless systems, it reduces to the *Vlasov* equation [21], which implies that the flow of stellar phase points through phase space is incompressible, or the density remains constant around a certain phase point [22]. This means that pressure has a negligible effect on the density of the fluid.

Accounting for these collisions would mean that we cannot model the interaction of a perturber with a gaseous fluid in the same way as Chandrasekhar did because we have assumed previously that only the perturber has gravitational influence on the whole system. Therefore, one must take the effects of *pressure* into consideration and use techniques from hydrodynamics to look into the effect of the presence of a perturber in a collisional fluid; and, in turn, look at the influence of the density perturbations induced on the perturber as a gaseous drag force, as we shall see in subsequent chapters. This was done by Ostriker [13] in the Newtonian case by analyzing the density perturbations induced by a gravitational potential on a collisional fluid with speed of sound c_s, through a Green's function analysis of the wave equation,

$$\nabla^2 \alpha - \frac{1}{c_s^2}\frac{\partial^2 \alpha}{\partial t^2} = -4\pi f(\mathbf{x}, t)$$

where α is the density perturbation function; and $c_s^2 f(\mathbf{x}, t)$ is the mass density of the fluid. This was obtained from linearized hydrodynamic equations describing an adiabatic gas influenced by a gravitational potential Φ_g. The gravitational drag induced by the density perturbation is then obtained by evaluating the volume integral,

$$F_{DF} = 2\pi G M_p \rho_o \int\int \mathrm{d}s \mathrm{d}R \; R \frac{\alpha(t) s}{(s^2 + R^2)^{3/2}}$$

which represents the interaction of the perturber and its induced wake. The following sections present the results of Ostriker, for perturbers in straight line motion, and Kim & Kim, for circular-orbit perturbers.

Ostriker (1999)

An extension to a case wherein the orbit is immersed on a collisional fluid was worked out by Dokuchaev [23], Ruderman & Spiegel [24], Raphaeli & Saltpeter [12], and Miller [25] in the heating and cooling of gas clouds in galactic encounters. Their findings imply that the gravitational drag is subdominant for cases wherein the perturber is at subsonic speed, because of the upwind and downwind symmetry of the wake induced; whereas, the supersonic case yields a counterpart that resembles that of the expression for the collisionless case.

However, with the time-depedent perturbation analysis presented by Ostriker [13], it was observed that the dynamical friction, however small, is nonzero. A subsonic perturber was observed to have induced a smoothly distributed elliptical density wake envelope centered at the perturber's position, with eccentricity $e = \mathcal{M}$, where $\mathcal{M}$ is the Mach number of the perturber. For a supersonic perturber, however, a density wake is induced within a Mach cone behind its trajectory, which has a half-opening angle $\theta = \arcsin\left(\frac{1}{\mathcal{M}}\right)$. This implies that the Mach cone disappears as the perturber's speed approach the subsonic regime.

It was noted that as the speed approaches the supersonic regime, the DF experienced by a moving body in a collisional system, approaches that of the collisionless case. However, for some values of the Mach number about the range $\sim 1.0 - 3.0$, the gaseous drag force has a stronger effect than its collisionless counterpart. Ostriker pointed out that this behavior implies that objects which were once far from the central mass can sink faster if they arrive at the gaseous regions before star formation, which will populate the region with stars corresponding to a collisionless system.

Kim & Kim (2007)

Although it was believed that Ostriker's result [13] exclusively works for the linear motion case, it was shown that it can be extended to the circular orbit case by Kim & Kim [14]. They were able to observe the density profiles of the fluid for different values of $\mathcal{M}$, and found out that for a perturber moving in subsonic speeds, the wake is distributed smoothly; while for the supersonic case, the tail seems to have a very sharp structure, signalling a sudden change, or a shock, in density near the perturber. The density wake bends toward the shape of the orbit which makes the dynamical friction effects asymmetric in its radial and azimuthal components. However, it is the region near the perturber, in which the overdensity is greatest, that contributes dominantly to the drag that it experiences due to the inverse-square nature of gravity.

The azimuthal component was found to be in agreement with the straight-line case by Ostriker in the subsonic case and peaks steeply at the range $\mathcal{M} \sim 1.2 - 1.4$.

However, the radial component of the gaseous drag appears to be subdominant for $\mathcal{M} < 1$, and becomes greater than the azimuthal component only for increasing Mach number from unity.

1.3 Relevance on extreme-mass-ratio inspirals

A compact object that gets caught by the gravitational influence of a much more massive object, such as a supermassive black hole (SMBH), loses energy in the form of gravitational wave (GW) emissions. These waves carry important information about the internal and external geometry of the central mass [26]. In 2015, the first direct detection of gravitational waves from a merger of a binary black hole system [27] began a new era of space science, that is gravitational wave astronomy. However, with the sensitivity of our ground-based detectors limited to observing systems with a total mass of a few hundred solar masses, plans are underway to launch observatories into space to detect GWs. The Laser Interferometer Space Antenna (LISA) is expected to have a sensitivity in the millihertz range which corresponds to a system with a total mass of $10^4 - 10^7$ solar masses [28]. The main source of gravitational wave detections of LISA will be massive black holes (MBH) in the galactic center, which is usually surrounded by stellar clusters, being a hotbed of star formation according to observation [29]. The capture of these stellar clusters by the MBHs, otherwise known as extreme-mass ratio inspirals (EMRI), is dominantly driven by the emission of GWs. The deviations of observed GW waveforms from the prediction of general relativity can give us an idea about the property of the medium in its surroundings, which usually affects the evolution of the orbit by accretion [30] or by dynamical friction [11, 31].

The possibility of probing the matter surrounding an EMRI was motivated by a series of papers of Chakrabarti, where it was shown that for extreme cases, the hydrodynamic interaction of an orbiting satellite with a supermassive black hole may force it to follow a stable orbit configuration. However, even below the extreme case posed by Chakrabarti, a significant distortion of the waveform templates can be induced. Narayan explored the possible strength of the hydrodynamic effect of a typical galactic nuclei environment on the orbit by estimating the torque exerted on an orbiting star due to the hydrodynamic interaction with the accretion disk via an advection-dominated flow (ADAF) [32]. He argued that majority of the inspiral events

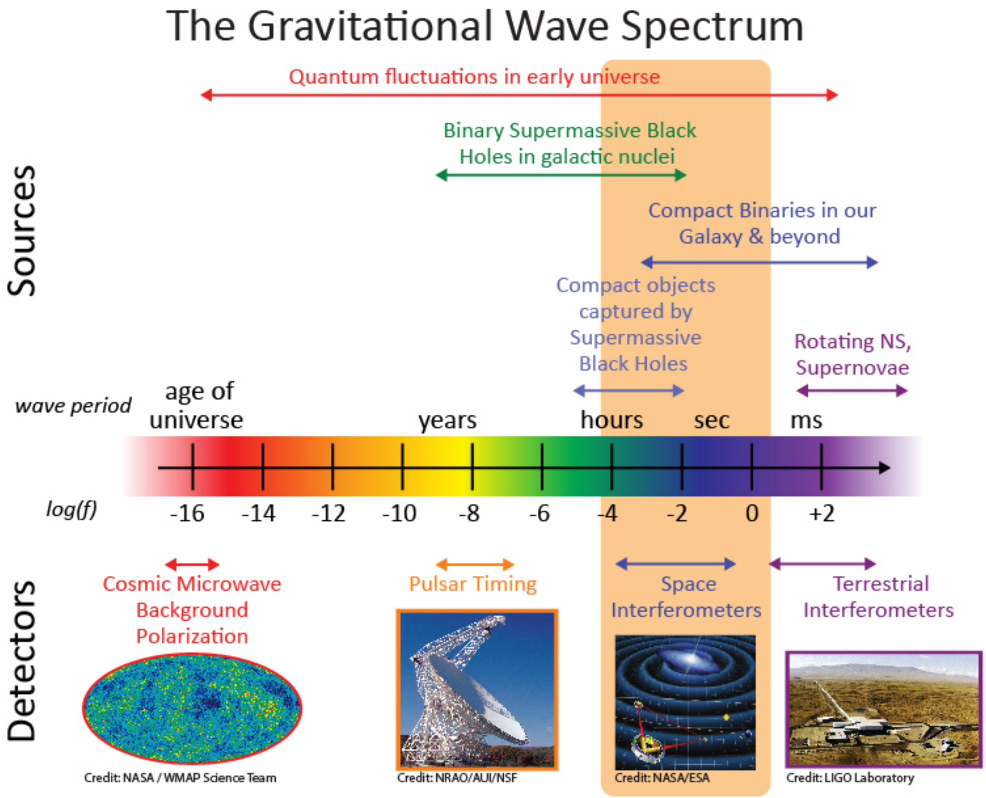

Figure 1.3: Detection techniques for events in space based on their frequency range. Compact objects captured by supermassive black holes (i.e. EMRIs) fall within a range that is not accessible to terrestrial detectors such as that of the observatories of the LIGO Collaboration. This prompts a space-based scheme in the form of the European Space Agency's Laser Interferometer Space Antenna (LISA) that is set to launch in 2034. Image downloaded from `https://lisa.nasa.gov/` in May 2018.

that LISA might detect will be unaffected by dynamical friction since the averaged number density of quasars, and the local number density of Seyfert galaxies, although numerous, are very low [32, 33, 34]. Further, since most observations on SMBH with sub-Eddington accretion are better explained by the ADAF model [35, 36, 37], Narayan mentioned that even if there were a thin disk around the SMBH, which is another self-consistent accretion flow solution [38], it will have been thousands of gravitational radius, R_g, away from the central black hole, thus subdominantly contributing any hydrodynamic drag on the orbiting satellite which is located within 10 R_g for gravitational wave experiments.

However, from a theoretical standpoint, Barausse pointed out that a study on the hydrodynamic drag induced for an EMRI is still worth considering for highly dense environments. For the case when the satellite crosses an accretion disk surrounding the central mass, an effective hydrodynamic drag may lead the satellite away from the predicted orbit. This was carried out by Subr and Karas, in a series of papers using both Newtonian and post-Newtonian analysis [39, 40], where they found out that, for thin disks, the disk-satellite interaction is dominant in EMRIs compared to that of the radiation reaction [41]. However, the first fully relativistic treatment for the interaction of an EMRI and an accretion disk was done by Barausse in Kerr spacetime. He found out that for cases when dynamical friction initially dominates over radiation reaction, the effect decays rapidly as it moves into the very-strong field region of the EMRI, thus proving it to be negligible in the later part of the inspiral [42].

While for most cases an astrophysical orbit may be approximated to be circular, studies on EMRIs usually deal with eccentric orbits [15, 43], which has not been attempted before for dynamical friction. This motivates the analysis of DF effects for a fully eccentric orbit. This study makes the first steps towards such a calculation. Instead of fully-eccentric orbits, we study orbits of small eccentricity.

1.4 Goals and delimitations

In this study, we formulate an analytic expression for the density wake induced by slightly eccentric immersed in tenuous fluid, by doing a perturbation analysis on the circular orbit case presented in Ref [16]. Density profiles for different velocity regimes (i.e. subsonic, transonic, and supersonic) are presented to observe the effect of the small eccentricity of the orbit on the density wakes formed by the perturber. Expressions for the metric perturbation are also derived to serve as a preliminary step to a complete calculation of the dynamical friction effects due to slightly eccentric orbits in collisional fluid.

We leave the calculation of dynamical friction for a slightly eccentric case for future work.

1.5 Outline of this manuscript

Through our previous discussion, we can now make sense of the problem that we wish to explore. The concept of dynamical friction gives us an idea as to how a homogeneous field of objects of a certain mass would affect a passing massive perturber.

Extending this to the relativistic case for slightly-eccentric orbits in collisional fluid may provide some insights about the behavior of EMRIs in highly dense gaseous environments like active galatic nuclei and Seyfert galaxies. A first step would be to explore the interaction of the moving body with its gaseous environment, which brings about a momentum loss.

In the next chapter, we discuss the relativistic extension by Barausse for calculating the dynamical friction effects in straight-line and circular particle orbits in the relativistic regime (Chapter 2). This serves as a main take-off point that we shall frequently return to in subsequent discussions.

Then, we propose an alternate way for solving the density perturbations over all space due to a perturber in a slightly eccentric orbit. We adopt techniques first employed in self-force calculations by Diaz-Rivera et al [44], and Apostolatos et al [45]. (Chapter 3)

Lastly, we generalize our findings and determine the significance of the perturbation introduced in the particle orbit in the context of Barausse's work. Future work on this topic is discussed. Possible extensions to this slightly-eccentric analysis are also presented. (Chapter 4)

Chapter 2

Barausse's relativistic extension to dynamical friction

In this chapter, we explore the mathematical preliminaries, and the methods employed by Barausse [16] to obtain the expression that describes the effect of dynamical friction on objects moving through a collisional system in flat spacetime.

Throughout the rest of this manuscript, we used units in which $G = c = 1$. This presentation of Barausse's results is faithful to the notation that he used in Ref [16].

2.1 Mathematical preliminaries

2.1.1 Metric and the stress-energy tensor

It is shown in the literature [46] that the metric of a flat spacetime with a perturber of mass M, moving through a perfect fluid at rest with density ρ and pressure p, can be written as a Minkowski background plus some perturbations, which has a general form,

$$d\tilde{s}^2 = \tilde{g}_{\mu\nu}\mathrm{d}x^\mu\mathrm{d}x^\nu = -(1+2\phi)\mathrm{d}t^2 + 2\omega_i\mathrm{d}x^i\mathrm{d}t + [\delta_{ij}(1-2\psi) + \chi_{ij}]\mathrm{d}x^i\mathrm{d}x^j \tag{2.1}$$

where ϕ and ψ are the perturbations to the metric. The three-vector component of the metric, ω_i, can be decomposed into its transverse (curl-free) and longitudinal (divergence-free) parts, such that

$$\omega_i = \partial_i\omega^{\parallel} + \omega_i^{\perp}, \qquad \partial_i\omega_i^{\perp} = 0 \tag{2.2}$$

and the traceless three-tensor χ_{ij} can be split into a trace part, a transverse part, and a longitudinal part, such that,

$$\chi_{ij} = D_{ij}\chi^{\parallel} + \partial_{(i}\chi^{\perp}_{j)} + \chi^{\top}_{ij}, \qquad \partial^i\chi^{\perp}_i = \partial^i\chi^{\top}_{ij} = \chi^{i\top}_i = 0 \tag{2.3}$$

where

$$D_{ij} \equiv \partial_i \partial_j - \frac{1}{3}\delta_{ij}, \qquad \nabla^2 = \delta^{ij}\partial_i\partial_j$$

In the same manner, the stress-energy tensor that corresponds to Equation (2.1) can be decomposed into

$$\begin{aligned} T_{\mu\nu}dx^\mu dx^\nu = T_{tt}dt^2 + 2(\partial_i S^{\parallel} + S_i^{\perp})\mathrm{d}t\mathrm{d}x^i \\ + \left[\frac{T}{3}\delta_{ij} + D_{ij}\Sigma^{\parallel} + \partial_{(i}\Sigma_{j)}^{\perp} + \Sigma_{ij}^{\top}\right]\mathrm{d}x^i\mathrm{d}x^j \end{aligned} \tag{2.4}$$

where

$$\partial^i S_i^{\perp} = \partial^i \Sigma_i^{\perp} = \partial^i \Sigma_{ij}^{\top} = \Sigma_i^{\top i} = 0$$

However, in order to closely follow the methods used by Ostriker and Kim & Kim, the Poisson gauge [47] ($\partial_i \omega^{\parallel} = \partial_i \chi^{ij}$) was chosen in Ref [16], such that in this gauge, the metric has the form,

$$d\tilde{s}^2 = -(1+2\phi)\mathrm{d}t^2 + 2\omega_i^{\perp}\mathrm{d}x^i\mathrm{d}t + [\delta_{ij}(1-2\psi) + \chi_{ij}^{\top}]\mathrm{d}x^i\mathrm{d}x^j \tag{2.5}$$

which gives a set of linearized Einstein equations relating the metric perturbations to the source terms:

$$\nabla^2\psi = 4\pi T_{tt} \tag{2.6}$$

$$\partial_t \psi = 4\pi S_{\parallel} \tag{2.7}$$

$$\nabla^2 \omega_i^{\perp} = -16\pi S_i^{\perp} \tag{2.8}$$

$$\nabla^2 \phi = 4\pi(T_{tt} + T) - 3\partial_t^2 \psi \tag{2.9}$$

$$\psi - \phi = 8\pi \Sigma^{\parallel} \tag{2.10}$$

$$\partial_t \omega_i^{\perp} = -8\pi \Sigma_i^{\perp} \tag{2.11}$$

$$\Box \chi_{ij}^{\top} = -16\pi \Sigma_{ij}^{\top} \tag{2.12}$$

where $\Box = \eta^{\mu\nu}\partial_\mu\partial_\nu$.

It is important to note that Barausse's perturbation analysis relies on two intrinsic error terms ε_1 and ε_2 that are induced by the presence of the fluid, $\varepsilon_1 \sim \mathcal{O}\left(\frac{\mathcal{L}}{\lambda_J}\right)$, and the moving perturber, $\varepsilon_2 \sim \mathcal{O}\left(\frac{M}{r_{min}}\right)$, where $\mathcal{L}$ is the characteristic size of the medium surrounding the orbit, λ_J is the generalized Jeans' length, which corresponds to the critical size of the medium before it gravitationally collapse. The cutoff radius r_{min} was introduced so as to keep the expansion ε_2 from diverging. The gravitational interaction of the field produced by the perturber and the fluid, gives rise to accretion onto the perturber, which also contributes to the drag and was already calculated for a Schwarzschild black hole moving through a homogeneous field of particles [11]. The gravitational interaction of the perturber to its own field, known as *self-force*, does not interfere with the effects of accretion onto the perturber and can be calculated separately [48].

2.1.2 Contribution of the perturber and the fluid

Ref [16] treats the contribution of the presence of the fluid from that of the perturber separately. The stress-energy tensor $T_{\mu\nu}$ was presented in terms of the individual contributions of the fluid and the perturber,

$$T_{\mu\nu} = T^{\text{pert}}_{\mu\nu} + T^{\text{fluid}}_{\mu\nu}$$

where $T^{\text{fluid}}_{\mu\nu}$ and $T^{pert}_{\mu\nu}$ represent the perturbed perfect fluid and, the moving perturber of mass M, respectively.

The stress-energy tensor of the fluid is given by a perturbed perfect fluid prescription,

$$T^{\text{fluid}}_{\mu\nu} = (\tilde{\rho} + \tilde{p})\tilde{u}_\mu \tilde{u}_\nu + \tilde{p}\tilde{g}_{\mu\nu} \tag{2.13}$$

where $\tilde{g}_{\mu\nu}$ is the metric in Poisson gauge, and the perturbed energy density, pressure, and four-velocity are defined as,

$$\tilde{\rho} = \rho + \delta\rho, \qquad \tilde{p} = p + \delta p \tag{2.14}$$

$$\tilde{u}_i = \delta u_i, \qquad \tilde{u}_t = -1 - \phi \tag{2.15}$$

where $\delta\rho$ and δp are small perturbations to the density and pressure respectively. The equation for $\tilde{u}_t$ is implied by the normalization condition, $\tilde{g}_{\mu\nu}\tilde{u}^\mu \tilde{u}^\nu = -1$, while the equation for $\tilde{u}_i$ came from the initial condition that the perfect fluid is at rest at the initial position of the perturber.

On the other hand, the stress-energy tensor prescribed for the point-mass perturber (see Ref [48], Equation 490) has the form

$$T^{\text{pert}}_{\mu\nu}(\mathbf{x}, t) = M \frac{\tilde{u}^{\text{pert}}_\mu \tilde{u}^{\text{pert}}_\nu}{\tilde{u}^t_{\text{pert}} \sqrt{-\det(\tilde{g})}} \delta^{(3)}[\mathbf{x} - \tilde{\mathbf{x}}_{\text{pert}}] \tag{2.16}$$

where $\tilde{\mathbf{x}}_{\text{pert}}$ and $\tilde{u}^{\text{pert}}_\mu$ are the perturbed trajectory and four-velocity, respectively. Expanding both quantities in terms of their unperturbed counterparts, while keeping in mind that the stress-energy tensor is intrinsically first-order because of the factor $M = r\varepsilon_2$, and considering that, $\det(\tilde{g}) = -(1 + 2\phi - 6\psi) \approx -1 + \mathcal{O}(\varepsilon_1, \varepsilon_2)$, the previous equation was written in a rather manageable form [16]

$$T^{\text{pert}}_{\mu\nu}(\mathbf{x}, t) = M \frac{u^{\text{pert}}_{\mu} u^{\text{pert}}_{\nu}}{u^{t}_{\text{pert}}} \delta^{(3)}[\mathbf{x} - \mathbf{x}_{\text{pert}}] \tag{2.17}$$

2.1.3 Obtaining the wave equation

It is expected that the total energy and baryon density of the system will still be conserved even after perturbations have been introduced to the system. Therefore, the continuity equation for a fluid, and the Euler equation must still hold in this case. Perturbing the the continuity equation,

$$\partial_\mu[\sqrt{-\det(\tilde{g})}\tilde{n}\tilde{u}^\mu] = 0$$

for a homogeneous background, where $\tilde{n} = n + \delta n$, the perturbed number density, yields an equation involving the density perturbation $\frac{\delta n}{n}$,

$$\begin{aligned} 0 &= \partial_\mu[\sqrt{-\det(\tilde{g})}\tilde{n}\tilde{u}^\mu] \\ &= -\frac{1}{2}\partial_\mu[\det(\tilde{g})][-\det(\tilde{g})]^{-\frac{1}{2}}\tilde{n}\tilde{u}^\mu + \sqrt{-\det(\tilde{g})}\tilde{u}^\mu\partial_\mu\tilde{n} + \sqrt{-\det(\tilde{g})}\tilde{n}\partial_\mu\tilde{u}^\mu \end{aligned}$$

By dropping the second order terms, we are left with,

$$\begin{aligned} 0 &= -\frac{1}{2}\partial_\mu[\det(\tilde{g})]\tilde{n}\tilde{u}^\mu + \tilde{u}^\mu\partial_\mu\tilde{n} + \tilde{n}\partial_\mu\tilde{u}^\mu \\ &= (\partial_\mu\phi - 3\partial_\mu\psi)\tilde{n}\tilde{u}^\mu + \tilde{u}^\mu\partial_\mu\left(\frac{\delta n}{n}\right) + \tilde{n}\partial_\mu\tilde{u}^\mu \\ &= -(\partial_t\phi - 3\partial_t\psi)(1+\phi)\tilde{n} - (1+\phi)\partial_t\left(\frac{\delta n}{n}\right) - \tilde{n}\partial_t\phi \\ &\qquad + (\partial_i\phi - 3\partial_i\psi)(\delta u^i)\tilde{n} - \delta u^i\partial_i\left(\frac{\delta n}{n}\right) + \tilde{n}\partial_i\delta u^i \\ &= \partial_t\left(\frac{\delta n}{n}\right) + \partial_i\delta u^i - 3\partial_t\psi \end{aligned} \tag{2.18}$$

On the other hand, perturbing the Euler equation,

$$\begin{aligned} \tilde{a}^\mu &= \tilde{u}^\alpha\tilde{\nabla}_\alpha\tilde{u}^\mu \\ &= -(\tilde{g}^{\mu\nu} + \tilde{u}^\mu\tilde{u}^\nu)\frac{\partial_\nu\tilde{h}}{\tilde{h}}, \qquad \tilde{h} \equiv \frac{(\tilde{p} + \tilde{\rho})}{\tilde{n}} = h + \delta h \ (\textit{perturbed specific enthalpy}) \end{aligned}$$

yields [16],

$$\partial_t \delta u^i + \partial_i \phi + \partial_t \omega_i^{\perp} + c_s^2 \partial_i \left(\frac{\delta n}{n} \right) = 0 \tag{2.19}$$

where c_s is the speed of sound in the fluid. Combining the gradient of Equation (2.19),

$$\begin{aligned} 0 &= \partial_i \partial_t \delta u^i + \nabla^2 \phi + \partial^i \partial_t \omega_i^{\perp} + c_s^2 \nabla^2 \left(\frac{\delta n}{n} \right) \\ &= \partial_i \partial_t \delta u^i + \nabla^2 \phi + c_s^2 \nabla^2 \left(\frac{\delta n}{n} \right), \qquad (\partial^i \omega_i^{\perp} = 0) \end{aligned}$$

where $\nabla^2 = \partial^i \partial_i$, and the time derivative of Equation (2.18),

$$\partial_t^2 \left(\frac{\delta n}{n} \right) + \partial_t \partial_i \delta u^i - 3 \partial_t^2 \psi = 0$$

gives us a differential wave equation for the density perturbation function $\frac{\delta n}{n}$

$$(\partial_t^2 - c_s^2 \nabla^2) \left(\frac{\delta n}{n} \right) - 3 \partial_t^2 \psi - \nabla^2 \phi = 0. \tag{2.20}$$

Substituting the linearized Einstein relation (2.9) to Equation (2.20) yields the wave equation in terms of the stress-energy of the sources,

$$(\partial_t^2 - c_s^2 \nabla^2) \left(\frac{\delta n}{n} \right) = 4\pi (T_{tt} + T) \tag{2.21}$$

which provides us with a clear picture of the relationship between the induced overdensities over all space and the presence of the fluid and the moving perturber. In the next section, we provide an outline of the application of this wave equation in the circular motion case studied by Barausse, which is the main interest of this study.

2.2 Perturbations induced for circular orbits

2.2.1 Baryon density perturbation

We consider a perturber moving along a circular orbit of radius R, with angular frequency Ω, such that its unperturbed four-velocity is given by,

$$u^{\mu}_{pert} \frac{\partial}{\partial x^{\mu}} = \gamma (\partial_t + \Omega \ \partial_\theta).$$

This trajectory cannot be maintained by *purely gravitational forces* in a flat spacetime background. Therefore, Barausse argued that for circular motion, the background spacetime must be necessarily curved, that is the spacetime should have a central Schwarzschild singularity immersed in a tenuous fluid at rest. Although physically inconsistent, the same metric as Equation (2.5) can be applied in the weak-field region of the spacetime, while neglecting the correction terms of order $\left(\frac{M_{BH}}{R_g}\right)$ due to the central singularity, where M_{BH} is the mass of the singularity, and R_g is the gravitational radius. Note that only for cases when R is close to M_{BH} can the perturber achieve relativistic speeds. Also, Barausse pointed out that this analysis still works out for dynamical friction by approximating the effect of the overdensities on the perturber to be restricted in its proximity, thus providing a good reason to work with the perturbed flat spacetime prescription as before. Proceeding with these assumptions, Equation (2.21) can then be rewritten in cylindrical coordinates (r, θ, z) as,

$$\begin{aligned}(\partial_t^2 - c_s^2\nabla^2)\left(\frac{\delta n}{n}\right) &= \frac{4\pi M\gamma(1+v^2)}{r}\delta(r-R)\delta(\theta-\Omega t)\delta(z)H(t) \\ &+ 4\pi[\rho(1+2\phi)+3p(1-2\psi)] + 4\pi(1+3c_s^2)(p+\rho)\frac{\delta n}{n}\end{aligned} \tag{2.22}$$

It was argued, however, that the latter expressions contribute error terms of order ε_1 due to the fact that a constant energy density and pressure, together with a flat spacetime background is not a solution to Einstein's equations, and of order $\varepsilon_J \sim \sqrt{\varepsilon_1}$, which is due to the Yukawa-like terms that arise from the contribution of the perturber on the $8\rho(\phi+3p\psi)$ term. In this approximation, the solution for [2.22] may be written as,

$$\frac{\delta n}{n}(\mathbf{x}, t) = f\frac{M\gamma(1+v^2)}{Rc_s^2}\mathcal{D}(\mathbf{x}, t) \times (1+\varepsilon_J) + \mathcal{O}\left(\frac{\mathcal{L}}{\lambda_J}\right) \tag{2.23}$$

where the weight function $\mathcal{D}(\mathbf{x}, t)$ is presented in Ref [14]. We emphasize that the main goal of this study is to obtain an equivalent expression for Equation (2.23) in the slightly eccentric case.

2.2.2 Metric perturbations

The metric perturbation $\delta g_{\mu\nu}$ in Equation (3.50) consist of a part contributed by the presence of the fluid, $\delta g_{\mu\nu}^{\text{fluid}}$, and by the moving perturber, $\delta g_{\mu\nu}^{\text{pert}}$. Substituting this to the Einstein field equation and splitting them according to each contribution yields [16],

$$\nabla^2\psi^{\text{pert}} = 8\pi\rho\phi^{\text{pert}} + 4\pi T_{tt}^{\text{pert}} \tag{2.24}$$

$$\nabla^2\psi^{\text{fluid}} = 4\pi\left[\rho + 2\rho\phi^{\text{fluid}} + (p+\rho)\frac{\delta n}{n}\right] \tag{2.25}$$

$$\psi^{\text{pert}} - \phi^{\text{pert}} = 8\pi\Sigma^{||}_{\text{pert}} \tag{2.26}$$

$$\psi^{\text{fluid}} - \phi^{\text{fluid}} = 0 \tag{2.27}$$

Substituting Equation (2.26) to Equation (2.24), gives us

$$\nabla^2\psi^{\text{pert}} = 8\pi\rho(\psi^{\text{pert}} - 8\pi\Sigma^{||}_{\text{pert}}) + 4\pi T^{\text{pert}}_{tt} \tag{2.28}$$

$$(\nabla^2 - 8\pi\rho)\psi^{\text{pert}} = 4\pi(T^{\text{pert}}_{tt} - 16\pi\rho\Sigma^{||}_{\text{pert}}) \tag{2.29}$$

which, by using the Green's function of the Yukawa operator $(\nabla^2 + \mu^2)$,

$$G(x) = \frac{\exp(-\mu|\mathbf{x}|)}{4\pi|\mathbf{x}|}$$

has a solution of the form

$$\psi^{\text{pert}}(\mathbf{x},t) = -\int d^3x' \frac{exp(-\sqrt{8\pi\rho}|\mathbf{x}-\mathbf{x}'|)}{|\mathbf{x}-\mathbf{x}'|}(T^{\text{pert}}_{tt} - 16\pi\rho\Sigma^{||}_{\text{pert}}) \tag{2.30}$$

whose gradient, as Barausse argues, contributes to the drag a term of order $\mathcal{O}(\rho M^2)$ which corresponds to the accretion onto the perturber.

We shift our focus to the contributions of the fluid on the drag. Doing the same procedure for the fluid contribution, gives a solution for the metric perturbation ψ^{fluid},

$$\psi^{\text{fluid}}(\mathbf{x},t) = -\int d^3x' \frac{exp(-\sqrt{8\pi\rho}|\mathbf{x}-\mathbf{x}'|)}{|\mathbf{x}-\mathbf{x}'|}\left[\rho + (\rho+p)\frac{\delta n}{n}(\mathbf{x'},t)\right] \tag{2.31}$$

whose derivative with respect to $\mathbf{x}$ gives

$$\partial_i\psi^{\text{fluid}}(\mathbf{x},t) = -\int d^3x' \frac{(\mathbf{x}-\mathbf{x}')\cdot\partial_i\mathbf{x}}{|\mathbf{x}-\mathbf{x}'|^3}\left[\rho + (\rho+p)\frac{\delta n}{n}(\mathbf{x}',t)\right](1+\varepsilon_{\text{Yukawa}}) \tag{2.32}$$

where $\varepsilon_{\text{Yukawa}}$ is the error term due to the expansion of the Yukawa potential. Note that this expression effectively has two contributing terms, one of which does not correspond to the effects of dynamical friction due to the induced overdensities. Then, the expression effectively reduces to,

$$\partial_i\psi^{\text{fluid}}(\mathbf{x},t) = -(\rho+p)\int d^3x' \frac{\delta n}{n}(\mathbf{x}',t)\frac{(\mathbf{x}-\mathbf{x}')\cdot\partial_i\mathbf{x}}{|\mathbf{x}-\mathbf{x}'|^3} \times (1+\varepsilon_{\text{Yukawa}}) + \varepsilon_{\text{notDF}} \tag{2.33}$$

2.2.3 Metric perturbations in t, r, ϕ, and z

Ref [16] evaluated the gradient of the metric perturbation due to each coordinate. We must recall that due to the symmetry of the system in the z-direction, the dynamical friction due to z has no resultant effect,

$$\partial_z \psi^{\text{fluid}} = \varepsilon_{\text{notDF}}. \tag{2.34}$$

On the other hand, the azimuthal and time gradients are given by,

$$\begin{aligned}\partial_\theta \psi^{\text{fluid}} = \partial_\theta \phi^{\text{fluid}} &= -\frac{\partial_t \psi^{\text{fluid}}}{\Omega} = -\frac{\partial_t \phi^{\text{fluid}}}{\Omega} && (2.35)\\ &= \frac{4\pi(p+\rho)M\gamma(1+v^2)R}{v^2} I_\theta \times [1+\mathcal{O}(\mathcal{L}/\lambda_J)] && (2.36)\end{aligned}$$

where the weight function I_θ is given by,

$$I_\theta \equiv -\frac{\mathcal{M}^2}{4\pi}\int d^3\hat{x}' \frac{\mathcal{D}(\mathbf{x}', t=\theta/\Omega)\hat{r}'\sin(\theta'-\theta)}{[1+\hat{z}'^2+\hat{r}'^2-2\hat{r}'\cos(\theta-\theta')]^{3/2}} \tag{2.37}$$

where the hat corresponds to a change of variables that is scaled to the radius of the perturber R, $\hat{x}' = \frac{x'}{R}$. In the same manner, the radial gradient of the metric perturbation has the form,

$$\partial_r \psi^{\text{fluid}} = \partial_r \phi^{\text{fluid}} = \frac{4\pi(p+\rho)M\gamma(1+v^2)R}{v^2} I_r \times [1+\mathcal{O}(\mathcal{L}/\lambda_J)] \tag{2.38}$$

where I_r is given by,

$$I_r \equiv -\frac{\mathcal{M}^2}{4\pi}\int d^3\hat{x}' \frac{\mathcal{D}(\mathbf{x}', t=\theta/\Omega)[\hat{r}'\cos(\theta'-\theta)-1]}{[1+\hat{z}'^2+\hat{r}'^2-2\hat{r}'\cos(\theta-\theta')]^{3/2}} \tag{2.39}$$

2.3 Summary and some remarks

Through a suitable choice of gauge, Barausse was able to provide a relativistic expression for the dynamical friction effects for a perturber in straight-line and circular motion by performing a linear perturbation on flat spacetime. Although inconsistent with physical considerations (that is, only straight-line motion can be maintained in flat spacetime), he was able to produce a description of the induced density wake akin to that of Kim & Kim, with a relativistic factor, which implies that the same but amplified effect on the fluid's density profile holds in the relativistic regime.

However, we should carefully note that this may not apply for a very massive perturber, where the linear perturbation analysis of Ostriker [13] and Kim & Kim

[14] may not apply. In another paper by Kim on the nonlinear effects of dynamical friction on very massive perturbers [49], the dynamical friction effects for a supersonic perturber was observed to be greater than its linear counterpart. For highly nonlinear cases, the drag force experienced by the perturber would be less than that of the linear case, which implies that the the process of dynamical friction would take longer than in the linear case. In this work, we restrict ourselves purely to the linear regime following the procedure done by Refs [13, 14, 16].

Chapter 3

Determining the density perturbation function $\frac{\delta n}{n}$

In the previous section, we explored the methods used by Barausse in solving for the DF effects on straight-line and circular orbits in a collisional fluid. It was observed that the results of Ref [13] and [14] still hold for velocities approaching the speed of light, given that a relativistic multiplicative factor is included in the expression, and that the rest-mass density is replaced with the pressure and energy density of the fluid [16].

However, knowing that studies on extreme-mass ratio inspirals often deal with eccentric orbits, an extension of Barausse's work to the slightly eccentric case may be of use in refining our understanding of DF on the evolution of EMRIs. In the remaining chapters of this manuscript, we present a *purely analytic* method for computing the perturbations induced by slightly eccentric orbits, thereby extending the previously presented methods by Barausse.

In this chapter, we propose an alternate method for solving for the density perturbation in the fluid, due to presence of a moving perturber. It is likewise assumed in this study that the use of a flat spactime background with some perturbations is apt in approximating the dynamics of circular orbits in a weakly-curved spacetime. We are aware that this is physically inconsistent because only straight line motion is allowed for particles set into motion by *purely gravitational forces* in a flat spacetime background. However, as discussed earlier, we can approximate the weak-field region of a perturbed Schwarzschild background as a perturbed Minkowski background, by neglecting errors of order $\left(\frac{M_{BH}}{R_g}\right)$. The particle and the fluid are also assumed to exist perpetually, that is we are already considering the steady-state behavior of the density wake for all cases. Also, we have limited our perturbation analysis to a linear order in δR.

3.1 Source decomposition for slightly eccentric orbits

We have previously encountered the wave equation for the density perturbation over all space, due to a perturber of mass M, moving along a circular orbit of radius R. To solve the wave equation for a slightly eccentric source, we adopt tehcniques first introduced by the self-force calculations of Apostolatos et al [45], and Diaz-Rivera et al [44]. In spherical coordinates, the wave equation is given by

$$(\partial_t^2 - c_s^2\nabla^2)\frac{\delta n}{n} = \frac{4\pi M\gamma(1+v^2)}{r^2\sin\theta}\delta(r-R(t))\delta\left(\theta-\frac{\pi}{2}\right)\delta(\phi-\Phi(t)) \tag{3.1}$$

where $v = \Omega_o r_o$, and in which $R(t)$ and $\Phi(t)$ may be expanded in powers of a small parameter δR,

$$R(t) = r_o + \delta R\cos(\Omega_r t) + \mathcal{O}(\delta R^2) \tag{3.2}$$

$$\Phi(t) = \Omega_o t + \frac{d\Omega_\phi}{dR}\frac{\delta R}{\Omega_r}\sin(\Omega_r t) + \mathcal{O}(\delta R^2) \tag{3.3}$$

where Ω_r and Ω_ϕ are the fundamental frequencies of radial and angular motion, respectively. The rate of change of the angular frequency with respect to a change in the radius is given by,

$$\frac{d\Omega_\phi}{dR} = -\frac{2}{r_o}\Omega_\phi \tag{3.4}$$

while the angular frequency is given by the time derivative of $\Phi(t)$

$$\begin{aligned}\Omega_\phi \equiv \frac{\mathrm{d}\Phi}{\mathrm{d}t} &= \Omega_o + \frac{d\Omega_\phi}{dR}\delta R\cos(\Omega_r t)\\ &= \Omega_o\left(1 - \frac{2\delta R\cos(\Omega_r t)}{r_o}\right)\end{aligned}$$

The next steps of the calculation require that we substitute these expressions to Equation (3.1) and expand $(r - R(t))$ about $(r - r_o)$, and $(\phi - \Phi(t))$ about $(\phi - \Omega_o t)$, thereby introducing derivatives of radial and azimuthal delta functions,

$$\begin{aligned}\delta(r - R(t)) &= \delta(r - r_o - \delta R\cos(\Omega_r t))\\ &\approx \delta(r - r_o) - \delta R\cos(\Omega_r t)\delta'(r - r_o)\\ \delta(\phi - \Phi(t)) &= \delta\left(\phi - \Omega_o t - \frac{d\Omega_\phi}{dR}\frac{\delta R}{\Omega_r}\sin(\Omega_r t)\right)\\ &\approx \delta(\phi - \Omega_o t) - \frac{d\Omega_\phi}{dR}\frac{\delta R}{\Omega_r}\sin(\Omega_r t)\delta'(\phi - \Omega_o t)\end{aligned}$$

while performing a spherical harmonic decomposition of the source, which includes an *integration by parts* on ϕ,

$$
\begin{aligned}
\rho_{lm} &= \oint \rho Y^*_{lm}(\theta,\phi) d\Omega \\
&= \oint \left\{ M\gamma(1+v^2)\delta(r-R(t))\delta\left(\theta-\frac{\pi}{2}\right)\delta(\phi-\Phi(t))\right\} Y^*_{lm}(\theta,\phi)\mathrm{d}\theta\mathrm{d}\phi \\
&= M\gamma(1+v^2)\delta(r-R(t)) \oint \delta\left(\theta-\frac{\pi}{2}\right)\delta(\phi-\Phi(t))Y^*_{lm}(\theta,\phi)\mathrm{d}\theta\mathrm{d}\phi \\
&= M\gamma(1+v^2)\delta(r-R(t)) \\
&\qquad \oint \left[\delta(\phi-\Omega_o t) - \frac{d\Omega_\phi}{dR}\frac{\delta R}{\Omega_r}\sin(\Omega_r t)\delta'(\phi-\Omega_o t)\right] Y^*_{lm}\left(\frac{\pi}{2},\phi\right)\mathrm{d}\phi \\
&= M\gamma(1+v^2)\delta(r-R(t)) \\
&\qquad \left\{Y^*_{lm}\left(\frac{\pi}{2},\Omega_o t\right) - imY^*_{lm}\left(\frac{\pi}{2},\Omega_o t\right)\frac{d\Omega_\phi}{dR}\frac{\delta R}{\Omega_r}\sin(\Omega_r t)\right\} \\
&= M\gamma(1+v^2)Y^*_{lm}\left(\frac{\pi}{2},\Omega_o t\right) \\
&\qquad [\delta(r-ro) - \delta R\cos(\Omega_r t)\delta'(r-ro)]\left[1 - im\frac{d\Omega_\phi}{dR}\frac{\delta R}{\Omega_r}\sin(\Omega_r t)\right]
\end{aligned}
$$

We can express the previously obtained decomposition of ρ in terms of exponential functions in order to reveal a frequency spectrum in terms of the harmonics of $\omega^o_m = m\Omega_o$, alongside two other sidebands at frequencies, $\omega^\pm_m = m\Omega_o \pm \Omega_r$.

$$
\begin{aligned}
\rho_{lm} &= M\gamma(1+v^2)Y^*_{lm}\left(\frac{\pi}{2},0\right)e^{-im\Omega_o t} \\
&\left[\delta(r-r_o) - \frac{\delta R}{2}(e^{i\Omega_r t}+e^{-i\Omega_r t})\delta'(r-r_o)\right]\left[1 - m\frac{\delta R}{2}\frac{d\Omega_\phi}{dR}\frac{1}{\Omega_r}(e^{i\Omega_r t}-e^{-i\Omega_r t})\right] \\
&= M\gamma(1+v^2)Y^*_{lm}\left(\frac{\pi}{2},0\right)e^{-im\Omega_o t}\Big[\delta(r-r_o) - \frac{\delta R}{2}(e^{i\Omega_r t}+e^{-i\Omega_r t})\delta'(r-r_o) \\
&\qquad - m\frac{\delta R}{2}\frac{d\Omega_\phi}{dR}\frac{1}{\Omega_r}(e^{i\Omega_r t}-e^{-i\Omega_r t})\delta(r-r_o) + \mathcal{O}(\delta R^2)\Big] \\
&= \left[M\gamma(1+v^2)Y^*_{lm}\left(\frac{\pi}{2},0\right)\delta(r-r_o)\right]e^{-im\Omega_o t} \\
&\qquad - \frac{\delta R}{2}\left[M\gamma(1+v^2)Y^*_{lm}\left(\frac{\pi}{2},0\right)\right] \\
&\qquad\qquad \left[\delta'(r-r_o) + m\delta(r-r_o)\frac{d\Omega_\phi}{dR}\frac{1}{\Omega_r}\right]e^{-i(m\Omega_o-\Omega_r)t} \\
&\qquad - \frac{\delta R}{2}\left[M\gamma(1+v^2)Y^*_{lm}\left(\frac{\pi}{2},0\right)\right] \\
&\qquad\qquad \left[\delta'(r-r_o) - m\delta(r-r_o)\frac{d\Omega_\phi}{dR}\frac{1}{\Omega_r}\right]e^{-i(m\Omega_o+\Omega_r)t} \\
&\qquad\qquad + \mathcal{O}(\delta R^2)
\end{aligned}
$$

Substituting Equation (3.4) to the previous expression gives us a source decomposition in terms of the angular frequency and orbital radius r_o,

$$\begin{aligned}
&\rho_{lm} = \left[M\gamma(1+v^2)Y^*_{lm}\left(\frac{\pi}{2},0\right)\delta(r-r_o)\right]e^{-im\Omega_o t} \\
&-\frac{\delta R}{2}\left[M\gamma(1+v^2)Y^*_{lm}\left(\frac{\pi}{2},0\right)\right]\left[\delta'(r-r_o)-m\delta(r-r_o)\frac{2}{r_o}\frac{\Omega_\phi}{\Omega_r}\right]e^{-i(m\Omega_o-\Omega_r)t} \\
&-\frac{\delta R}{2}\left[M\gamma(1+v^2)Y^*_{lm}\left(\frac{\pi}{2},0\right)\right]\left[\delta'(r-r_o)+m\delta(r-r_o)\frac{2}{r_o}\frac{\Omega_\phi}{\Omega_r}\right]e^{-i(m\Omega_o+\Omega_r)t}
\end{aligned} \tag{3.5}$$

which yields a source decomposition in terms of the fundamental frequencies of the orbit,

$$\rho = \sum_{\omega}\sum_{lm}\rho^{\omega}_{lm}e^{-i\omega t}Y_{lm}(\theta,\phi)$$

where $l = 0, ..., i$, $m = -l, ..., l$, and $\omega = \{\omega^o_m, \omega^{\pm}_m, \omega^{2\pm}_m\}$

3.2 Solving the wave equation

We proceed in solving the wave equation by performing *separation of variables* in spherical coordinates, where

$$\frac{\delta n}{n}(\mathbf{r},t) = \Psi(\mathbf{r},t) = \sum_{\omega=\omega_o,\omega_\pm}\sum_{l=0}^{\infty}\sum_{m=-l}^{l}\left[\Psi^{\omega}_{lm}(r)e^{-i\omega t}Y_{lm}(\theta,\phi)\right]$$

which, by substituting back to the wave equation, yields a purely radial equation for each l mode at a frequency ω,

$$\begin{aligned}
&\left[\partial_t^2 - c_s^2\left(\frac{1}{r^2}\frac{\partial}{\partial r}\left(r^2\frac{\partial}{\partial r}\right)+\frac{1}{r^2\sin^2\phi}\frac{\partial^2}{\partial\theta^2}+\frac{1}{r^2\sin\phi}\frac{\partial}{\partial\phi}\left(\sin\phi\frac{\partial}{\partial\phi}\right)\right)\right] \\
&\qquad\left[\Psi^{\omega}_{lm}(r)e^{-i\omega t}Y_{lm}(\theta,\phi)\right] \\
&\qquad = 4\pi\rho^{\omega}_{lm}e^{-i\omega t}Y_{lm}(\theta,\phi)
\end{aligned}$$

$$\begin{aligned}
&\Psi^{\omega}_{lm}Y_{lm}e^{-i\omega t}(-\omega^2) - \frac{c_s^2 e^{-i\omega t}Y_{lm}}{r^2}\left[2r\frac{d\Psi^{\omega}_{lm}}{dr}+r^2\frac{d^2\Psi^{\omega}_{lm}}{dr^2}\right] \\
&\qquad - c_s^2\Psi^{\omega}_{lm}e^{-i\omega t}\left(-\frac{l(l+1)}{r^2}Y_{lm}\right) \\
&\qquad = 4\pi\rho^{\omega}_{lm}e^{-i\omega t}Y_{lm}(\theta,\phi)
\end{aligned}$$

$$\frac{\mathrm{d}^2\Psi^{\omega}_{lm}}{\mathrm{d}r^2}+\frac{2}{r}\frac{\mathrm{d}\Psi^{\omega}_{lm}}{\mathrm{d}r}+\left(\left(\frac{\omega}{c_s}\right)^2-\frac{l(l+1)}{r^2}\right)\Psi^{\omega}_{lm} = -\frac{4\pi\rho^{\omega}_{lm}}{c_s^2} \tag{3.6}$$

We can also decompose our wavefunction solution in the same manner as we did for the source,

$$\Psi(\mathbf{r},t) = \sum_{l,m} \left(\Psi^{o}_{lm} e^{-i\omega_o t} + \delta R \chi^{+}_{lm} e^{-i\omega_+ t} + \delta R \chi^{-}_{lm} e^{-i\omega_- t}\right) Y_{lm}(\theta,\phi) \tag{3.7}$$

such that for each l mode, we obtain three second-order ordinary differential equations involving each of the frequencies.

In order to solve these differential equations, one must first solve the homogeneous case, then completely determine all remaining degrees of freedom by imposing regularity conditions and jump conditions due to the source. There are two regular points at $r = 0$ and at infinity, respectively. We must impose regularity at the origin, and expect that, at infinity, the solution approaches a outward going plane wave behavior that decays by $\frac{1}{r}$. We discuss the solution for each frequency separately, and deal with the whole solution by the end of this section.

3.2.1 Continuity and jump conditions

This subsection is a mathematical aside that presents an outline of the jump conditions at the boundary, $r = r_o$, that the wavefunction solution must satisfy.

We must first write the solution of our wave equation Ψ in the form,

$$\Psi = \Psi_- \Theta(r - r_o) + \Psi_+ \Theta(r_o - r) \tag{3.8}$$

where Θ is the Heaviside distribution, which manifestly tells us that Ψ_+ and Ψ_+ are the solutions inside and outside the orbital radius, respectively. Feeding Equation (3.8) to our radial differential equation yields an expression involving the delta function $\delta(r)$ and its derivative,

$$\begin{aligned} -\frac{4\pi\rho^{\omega}_{lm}}{c_s^2} = \Theta(r - r_o)\Big\{ &\left(\frac{\mathrm{d}^2\Psi_+}{\mathrm{d}r^2} - \frac{\mathrm{d}^2\Psi_-}{\mathrm{d}r^2}\right) + \frac{2}{r}\left(\frac{\mathrm{d}\Psi_+}{\mathrm{d}r} - \frac{\mathrm{d}\Psi_-}{\mathrm{d}r}\right) \\ &+ \left[\left(\frac{\omega}{c_s}\right)^2 - \frac{l(l+1)}{r^2}\right](\Psi_+ - \Psi_-)\Big\} \\ &+ \delta(r - r_o)\left\{2\left(\frac{\mathrm{d}\Psi_+}{\mathrm{d}r} - \frac{\mathrm{d}\Psi_-}{\mathrm{d}r}\right) + \frac{2}{r}(\Psi_+ - \Psi_-)\right\} \\ &+ \delta'(r - r_o)(\Psi_+ - \Psi_-) \end{aligned} \tag{3.9}$$

which, in order to obtain the jump conditions, must be matched with the source terms that we have previously computed.

Case 1: $\omega = \omega_o$

The source term due to the main frequency, from (3.5), is given by

$$\rho^{\omega_o}_{lm} = M\gamma(1+v^2)Y^*_{lm}\left(\frac{\pi}{2},0\right)\delta(r-r_o). \tag{3.10}$$

Plugging (3.10) into (3.9) yields a set of equations involving the relationship between the solutions inside and outside the orbital radius, and its derivatives,

$$\begin{cases} \left(\Psi^o_{lm,+} - \Psi^o_{lm,-}\right)\Big|_{r_o} = 0 \\ \left(\frac{\mathrm{d}\Psi^o_{lm,+}}{\mathrm{d}r} - \frac{\mathrm{d}\Psi^o_{lm,-}}{\mathrm{d}r}\right)\Big|_{r_o} = -\frac{2\pi M\gamma(1+v^2)Y^*_{lm}\left(\frac{\pi}{2},0\right)}{c_s^2} \end{cases} \tag{3.11}$$

which serve as our jump conditions for the solution of our wave equation for the main frequency. The jump conditions imply that the main frequency solution must be *continuous* at the boundary, but the derivatives from inside and outside the radius must not agree with each other.

Case 2: $\omega = \omega_\pm$

The source term due to the sideband frequencies is given by,

$$\rho^{\omega_\pm}_{lm} = -\frac{\delta R}{2}\left[M\gamma(1+v^2)Y^*_{lm}\left(\frac{\pi}{2},0\right)\right]\left[\delta'(r-r_o) \pm m\delta(r-r_o)\frac{2}{r_o}\frac{\Omega_\phi}{\Omega_r}\right] \tag{3.12}$$

Doing the same procedure as the first case, we obtain the relationship between the solutions inside and outside the orbital radius, and its derivatives,

$$\begin{cases} \left(\chi^\pm_{lm,+} - \chi^\pm_{lm,-}\right)\Big|_{r_o} = \frac{2\pi M\gamma(1+v^2)Y^*_{lm}\left(\frac{\pi}{2},0\right)}{c_s^2} \\ \left(\frac{\mathrm{d}\chi^\pm_{lm,+}}{\mathrm{d}r} - \frac{\mathrm{d}\chi^\pm_{lm,-}}{\mathrm{d}r}\right)\Big|_{r_o} = -\frac{2\pi M\gamma(1+v^2)Y^*_{lm}\left(\frac{\pi}{2},0\right)}{r_o c_s^2}\left(1 \pm m\frac{\Omega_o}{\Omega_r}\right) \end{cases} \tag{3.13}$$

and find out that the introduction of the derivative of a delta function $\delta'(r)$, being more singular than just a delta function, as a source term imposes a discontinuity in both the wavefunction solutions inside and outside the orbital radius, and their derivatives.

3.2.2 Solving the wave equation for ω_o

Our solution for the wave equation involving ω_o is divided for cases when $l, m = 0$, $l \neq 0, m = 0$, and $l, m \neq 0$. Solutions involving $m = 0$ correspond to a *static* case, which is fundamentally different from the problem when $m \neq 0$.

Case 1 : $l, m = 0$

For the case when $l, m = 0$, our wave equation assumes the form,

$$\frac{\mathrm{d}^2\Psi^o_{lm}}{\mathrm{d}r^2} + \frac{2}{r}\frac{\mathrm{d}\Psi^o_{lm}}{\mathrm{d}r} = -\frac{4\pi\rho^{\omega^o_m}_{lm}}{c_s^2}$$

which, in the homogeneous case, has a general solution inside and outside the orbital radius,

$$\Psi^o_{lm} = \begin{cases} -\frac{A}{r} + B, & r < r_o \\ -\frac{C}{r} + D, & r > r_o \end{cases}$$

In order for the solution to be defined at $r = 0$, we must impose the condition that $A = 0$. At infinity, we expect the wavefunction to vanish, thus prompting us to impose the condition that $D = 0$. This leaves us with two remaining degrees of freedom to determine by imposing the continuity and jump conditions. The continuity of the wavefunction at the boundary implies that

$$C_{00} = -B_{00} r_o \tag{3.14}$$

while the jump condition for this case is given by,

$$\frac{C_{00}}{r_o^2} = \frac{2\pi M\gamma(1+v^2)Y^*_{00}\left(\frac{\pi}{2},0\right)}{c_s^2} \rightarrow \boxed{C_{00} = \frac{2\pi M r_o^2\gamma(1+v^2)Y^*_{00}\left(\frac{\pi}{2},0\right)}{c_s^2}} \tag{3.15}$$

Substituting Equation (3.15) to Equation (3.14) gives us an expression for B,

$$\boxed{B_{00} = -\frac{2\pi M r_o\gamma(1+v^2)Y^*_{00}\left(\frac{\pi}{2},0\right)}{c_s^2}} \tag{3.16}$$

Case 2 : $l \neq 0,\ m = 0$

For cases when $l \neq 0,\ m = 0$, our wave equation assumes the form

$$\frac{\mathrm{d}^2\Psi^o_{lm}}{\mathrm{d}r^2} + \frac{2}{r}\frac{\mathrm{d}\Psi^o_{lm}}{\mathrm{d}r} - \frac{l(l+1)}{r^2}\Psi^\omega_{lm} = -\frac{4\pi\rho^\omega_{lm}}{c_s^2}$$

which has a general solution of the form,

$$\Psi^o_{lm} = \begin{cases} Ar^l + Br^{-(l+1)}, & r < r_o \\ Cr^l + Dr^{-(l+1)}, & r > r_o \end{cases}$$

Imposing regularity at $r = 0$ yields the condition that $B = 0$. For the solution not to diverge at infinity, $C = 0$. This leaves us with A and D to determine through the continuity and jump conditions. The continuity condition implies that

$$D_l = A_l r_o^{2l+1} \tag{3.17}$$

while the jump condition yields,

$$-(l+1)D_l r_o^{-l} - lA_l r_o^{l+1} = -\frac{2\pi M\gamma(1+v^2)Y_{l0}^*\left(\frac{\pi}{2},0\right)}{c_s^2} \tag{3.18}$$

Substituting Equation (3.17) to Equation(3.18) gives us an expression for A_l and D_l,

$$\boxed{A_l = \left[\frac{1}{(2l+1)r_o^{l+1}}\right]\frac{2\pi M\gamma(1+v^2)Y_{l0}^*\left(\frac{\pi}{2},0\right)}{c_s^2}} \tag{3.19}$$

$$\boxed{D_l = \left[\frac{r_o^l}{(2l+1)}\right]\frac{2\pi M\gamma(1+v^2)Y_{l0}^*\left(\frac{\pi}{2},0\right)}{c_s^2}} \tag{3.20}$$

Case 3 : $l, m \neq 0$

In cases when both l and m are non-zero, the wave equation has a general solution that is a combination of spherical Bessel functions of the first and second kind, j_l and n_l inside, and spherical Hankel functions of the first and second kind, $h_l^{(1)}$ and $h_l^{(2)}$, outside,

$$\Psi_{lm}^o = \begin{cases} Aj_l(\frac{\omega_m^o}{c_s}r) + Bn_l(\frac{\omega_m^o}{c_s}r) & r < r_o \\ Ch_l^{(1)}(\frac{\omega_m^o}{c_s}r) + Dh_l^{(2)}(\frac{\omega_m^o}{c_s}r) & r > r_o \end{cases}$$

For the solution to be regular at $r = 0$, $B = 0$ because the Neumann function diverges at zero. We expect that at infinity, the wavefunction behaves as an outgoing plane wave that decays by $1/r$, which implies that $D = 0$ because the spherical Hankel function of the second kind represents ingoing plane waves. Again, this leaves us with A and C to determine through the continuity and jump conditions. The continuity condition yields a relationship between A and C of the form,

$$C_{lm} = A_{lm}\frac{j_l\left(\frac{\omega_m^o}{c_s}r_o\right)}{h_l\left(\frac{\omega_m^o}{c_s}r_o\right)} \tag{3.21}$$

while the jump condition yields

$$\left\{\frac{C_{lm}}{2}\left(\frac{\omega_m^o}{c_s}\right)\left[(h_{l-1}^{(1)} - h_{l+1}^{(1)}) - \frac{h_l^{(1)}}{r_o}\right] - \frac{A_{lm}}{2}\left(\frac{\omega_m^o}{c_s}\right)\left[(j_{l-1} - j_{l+1}) - \frac{j_l}{r_o}\right]\right\}$$
$$= -\frac{2\pi M\gamma(1+v^2)Y_{lm}^*\left(\frac{\pi}{2},0\right)}{c_s^2} \tag{3.22}$$

where $h^{(1)}_{l-1}, h^{(1)}_{l+1}, h^{(1)}_l, j_{l-1}, j_{l+1},$ and j_l are evaluated at $r = r_o$. Substituting Equation (3.21) to Equation (3.22), completely determines the remaining constants

$$\begin{aligned}
-\frac{2\pi M\gamma(1+v^2)Y^*_{lm}\left(\frac{\pi}{2},0\right)}{c_s^2} &= \left(\frac{\omega^o_m}{c_s}\right)\left\{\frac{A_{lm}}{2}\left[\left(\frac{h^{(1)}_{l-1}-h^{(1)}_{l+1}}{h^{(1)}_l}\right)j_l - \frac{j_l}{r_o}\right]\right. \\
&\qquad\qquad \left. - \frac{A_{lm}}{2}\left[(j_{l-1}-j_{l+1}) - \frac{j_l}{r_o}\right]\right\} \\
&= A_{lm}\frac{\omega^o_m\mathcal{M}}{2v}\left[\left(\frac{h^{(1)}_{l-1}-h^{(1)}_{l+1}}{h^{(1)}_l}\right)j_l - (j_{l-1}-j_{l+1})\right]
\end{aligned}$$

$$A_{lm} = \frac{-2\pi M\gamma(1+v^2)Y^*_{lm}\left(\frac{\pi}{2},0\right)}{f^o_{lm}(r_o)}, \qquad C_{lm} = \frac{-2\pi M\gamma(1+v^2)Y^*_{lm}\left(\frac{\pi}{2},0\right)}{g^o_{lm}(r_o)} \tag{3.23}$$

where

$$\begin{aligned}
f^o_{lm}(r_o) &= \frac{\omega^o_m v}{2\mathcal{M}}\left[\left(\frac{h^{(1)}_{l-1}-h^{(1)}_{l+1}}{h^{(1)}_l}\right)j_l - (j_{l-1}-j_{l+1})\right]\Bigg|_{r_o} \\
g^o_{lm}(r_o) &= \frac{\omega^o_m v}{2\mathcal{M}}\left[\left(\frac{j_{l-1}-j_{l+1}}{j_l}\right)h^{(1)}_l - (h^{(1)}_{l-1}-h^{(1)}_{l+1})\right]\Bigg|_{r_o}
\end{aligned} \tag{3.24}$$

and $\mathcal{M}$ is the Mach number of the perturber, which is taken to be the ratio between the velocity of the perturber and the speed of sound in the fluid $\left(\mathcal{M} = \frac{v}{c_s}\right)$. Recasting our expressions to a form where the Mach number manifest is important in our analysis since we are dealing with collisional fluids.

3.2.3 Solving the wave equation for $\omega^{\pm}_m$

Since we are solving the same wave equation for the sidebands as the third case for ω_o, the solution that we have previously acquired also applies for the rest of the frequencies. The only difference between the solutions is the jump condition that they must satisfy. Proceeding in the same manner as in the third case for ω_o, we obtain solutions for $\omega^{\pm}_m$ of the form,

$$\chi^{\pm}_{lm} = \begin{cases} A^{\pm}_{lm} j_l\left(\frac{\omega^{\pm}_m}{c_s}r\right) & r < r_o \\ C^{\pm}_{lm} h^{(1)}_l\left(\frac{\omega^{\pm}_m}{c_s}r\right) & r > r_o \end{cases}$$

The jump condition for the wavefunction solutions for the sideband frequencies gives us an expression for $C^{\pm}_{lm}$ in terms of $A^{\pm}_{lm}$,

$$C^{\pm}_{lm} = \frac{2\pi M\gamma(1+v^2)Y^*_{lm}\left(\frac{\pi}{2},0\right)}{c_s^2 h^{(1)}_l\left(\frac{\omega^{\pm}_m}{c_s}r_o\right)} + A^{\pm}_{lm}\frac{j_l\left(\frac{\omega^{\pm}_m}{c_s}r_o\right)}{h^{(1)}_l\left(\frac{\omega^{\pm}_m}{c_s}r_o\right)} \tag{3.25}$$

while the jump condition for the derivatives yields,

$$\left\{\frac{C^{\pm}_{lm}}{2}\left(\frac{\omega^{\pm}_{m}}{c_s}\right)\left[(h^{(1)}_{l-1}-h^{(1)}_{l+1})-\frac{h^{(1)}_{l}}{r_o}\right]-\frac{A^{\pm}_{lm}}{2}\left(\frac{\omega^{\pm}_{m}}{c_s}\right)\left[(j_{l-1}-j_{l+1})-\frac{j_l}{r_o}\right]\right\}$$
$$=-\frac{2\pi M\gamma(1+v^2)Y^{*}_{lm}\left(\frac{\pi}{2},0\right)}{r_o c_s^2}\left(1\pm m\frac{\Omega_o}{\Omega_r}\right). \qquad (3.26)$$

By substituting (3.25) to (3.26), we obtain an expression for the coefficients of the form,

$$A^{\pm}_{lm}=-\frac{2\pi M\gamma(1+v^2)Y^{*}_{lm}\left(\frac{\pi}{2},0\right)}{c_s^2}f^{\pm}_{lm}(r_o) \qquad (3.27)$$

$$C^{\pm}_{lm}=\frac{2\pi M\gamma(1+v^2)Y^{*}_{lm}\left(\frac{\pi}{2},0\right)}{c_s^2}g^{\pm}_{lm}(r_o) \qquad (3.28)$$

where

$$f^{\pm}_{lm}(r_o)=\frac{\left(1\pm 2m\frac{\Omega_o}{\Omega_r}\right)+\frac{\omega^{\pm}_{m}}{c_s}\left(\frac{h^{(1)}_{l-1}-h^{(1)}_{l+1}}{h^{(1)}_{l}}\right)\Big|_{r_o}}{\frac{\omega^{\pm}_{m}v}{2\mathcal{M}}\left[\left(\frac{h^{(1)}_{l-1}-h^{(1)}_{l+1}}{h^{(1)}_{l}}\right)j_l-(j_{l-1}-j_{l+1})\right]\Big|_{r_o}}$$

$$g^{\pm}_{lm}(r_o)=\frac{1}{h^{(1)}_{l}\left(\frac{\omega^{\pm}_{m}}{c_s}r_o\right)}-\frac{\left(1\pm 2m\frac{\Omega_o}{\Omega_r}\right)+\frac{\omega^{\pm}_{m}}{c_s}\left(\frac{h^{(1)}_{l-1}-h^{(1)}_{l+1}}{h^{(1)}_{l}}\right)\Big|_{r_o}}{\frac{\omega^{\pm}_{m}v}{2\mathcal{M}}\left[\left(h^{(1)}_{l-1}-h^{(1)}_{l+1}\right)-h^{(1)}_{l}(\frac{j_{l-1}-j_{l+1}}{j_l})\right]\Big|_{r_o}}$$

3.2.4 In Brief

In summary, we were able to solve Equation (3.1) by means of separation of variables, through a spherical decomposition of the source that revealed an explicit discontinuity in the radial component of the solution due the sideband frequency contributions due to its very singular nature. The following jump conditions were obtained

$$\begin{cases}(\Psi^{o}_{lm,+}-\Psi^{o}_{lm,-})\Big|_{r_o}=0\\ \left(\frac{\mathrm{d}\Psi^{o}_{lm,+}}{\mathrm{d}r}-\frac{\mathrm{d}\Psi^{o}_{lm,-}}{\mathrm{d}r}\right)\Big|_{r_o}=-\frac{2\pi M\gamma(1+v^2)Y^{*}_{lm}\left(\frac{\pi}{2},0\right)}{c_s^2}\end{cases}$$

$$\begin{cases}(\chi^{\pm}_{lm,+}-\chi^{\pm}_{lm,-})\Big|_{r_o}=\frac{2\pi M\gamma(1+v^2)Y^{*}_{lm}\left(\frac{\pi}{2},0\right)}{c_s^2}\\ \left(\frac{\mathrm{d}\chi^{\pm}_{lm,+}}{\mathrm{d}r}-\frac{\mathrm{d}\chi^{\pm}_{lm,-}}{\mathrm{d}r}\right)\Big|_{r_o}=-\frac{2\pi M\gamma(1+v^2)Y^{*}_{lm}\left(\frac{\pi}{2},0\right)}{r_o c_s^2}\left(1\pm m\frac{\Omega_o}{\Omega_r}\right)\end{cases}$$

by writing the solution in the form,

$$\Psi=\Psi_{-}\Theta(r_o-r)+\Psi_{+}\Theta(r-r_o)$$

feeding it back to the wave equation, and matching the coefficients of the delta function and its derivative with their counterparts in the source terms. These jump conditions yield the coefficients in the solutions inside and outside the orbital radius,

$$
\begin{aligned}
\Psi_{in}(\mathbf{x},t) &= \Psi^{o}_{lm,-} + \chi^{+}_{lm,-} + \chi^{-}_{lm,-} \\
&= \sum_{l,m\neq o} A_{lm} j_l\left(\frac{\omega^{o}_{m}}{c_s}r\right) e^{-i\omega^{o}_{m}t} Y_{lm}(\theta,\phi) + \sum_{l,m} A^{+}_{lm} j_l\left(\frac{\omega^{+}_{m}}{c_s}r\right) e^{-i\omega^{+}_{m}t} Y_{lm}(\theta,\phi) \\
&\quad + \sum_{l,m} A^{-}_{lm} j_l\left(\frac{\omega^{-}_{m}}{c_s}r\right) e^{-i\omega^{-}_{m}t} Y_{lm}(\theta,\phi) + \sum_{l} A_l r^{l} Y_{l0}(\theta,\phi) + B_{00} Y_{00}(\theta,\phi) \\
\Psi_{out}(\mathbf{x},t) &= \Psi^{o}_{lm,+} + \chi^{+}_{lm,+} + \chi^{-}_{lm,+} \\
&= \sum_{l,m\neq o} C_{lm} h^{(1)}_l\left(\frac{\omega^{o}_{m}}{c_s}r\right) e^{-i\omega^{o}_{m}t} Y_{lm}(\theta,\phi) + \sum_{l,m} C^{+}_{lm} h^{(1)}_l\left(\frac{\omega^{+}_{m}}{c_s}r\right) e^{-i\omega^{+}_{m}t} Y_{lm}(\theta,\phi) \\
&\quad + \sum_{l,m} C^{-}_{lm} h^{(1)}_l\left(\frac{\omega^{-}_{m}}{c_s}r\right) e^{-i\omega^{-}_{m}t} Y_{lm}(\theta,\phi) + \sum_{l} A_l r^{-1(l+1)} Y_{l0}(\theta,\phi) - \frac{C_{00}}{r} Y_{00}(\theta,\phi)
\end{aligned}
$$

where

$$
\begin{aligned}
A_l &= \left[\frac{1}{(2l+1)r_o^{l+1}}\right]\frac{2\pi M\gamma(1+v^2)Y^{*}_{l0}\left(\frac{\pi}{2},0\right)}{c_s^2} & D_l &= \left[\frac{r_o^{l}}{(2l+1)}\right]\frac{2\pi M\gamma(1+v^2)Y^{*}_{l0}\left(\frac{\pi}{2},0\right)}{c_s^2} \\
B_{00} &= -\frac{2\pi M r_o\gamma(1+v^2)Y^{*}_{00}\left(\frac{\pi}{2},0\right)}{c_s^2} & C_{00} &= \frac{2\pi M r_o^2\gamma(1+v^2)Y^{*}_{00}\left(\frac{\pi}{2},0\right)}{c_s^2} \\
A_{lm} &= \frac{-2\pi M\gamma(1+v^2)Y^{*}_{lm}\left(\frac{\pi}{2},0\right)}{f^{o}_{lm}(r_o)} & C_{lm} &= \frac{-2\pi M\gamma(1+v^2)Y^{*}_{lm}\left(\frac{\pi}{2},0\right)}{g^{o}_{lm}(r_o)} \\
A^{\pm}_{lm} &= -\frac{2\pi M\gamma(1+v^2)Y^{*}_{lm}\left(\frac{\pi}{2},0\right)}{c_s^2} f^{\pm}_{lm}(r_o) & C^{\pm}_{lm} &= \frac{2\pi M\gamma(1+v^2)Y^{*}_{lm}\left(\frac{\pi}{2},0\right)}{c_s^2} g^{\pm}_{lm}(r_o)
\end{aligned}
$$

$$
\begin{aligned}
f^{o}_{lm}(r_o) &= \frac{\omega^{o}_{m}v}{2\mathcal{M}}\left[\left(\frac{h^{(1)}_{l-1}-h^{(1)}_{l+1}}{h^{(1)}_{l}}\right) j_l - (j_{l-1}-j_{l+1})\right]\Big|_{r_o} \\
g^{o}_{lm}(r_o) &= \frac{\omega^{o}_{m}v}{2\mathcal{M}}\left[\left(\frac{j_{l-1}-j_{l+1}}{j_l}\right) h^{(1)}_l - (h^{(1)}_{l-1}-h^{(1)}_{l+1})\right]\Big|_{r_o}
\end{aligned}
$$

$$
\begin{aligned}
f^{\pm}_{lm}(r_o) &= \frac{\left(1\pm 2m\frac{\Omega_o}{\Omega_r}\right) + \frac{\omega^{\pm}_{m}}{c_s}\left(\frac{h^{(1)}_{l-1}-h^{(1)}_{l+1}}{h^{(1)}_{l}}\right)\Big|_{r_o}}{\frac{\omega^{\pm}_{m}v}{2\mathcal{M}}\left[\left(\frac{h^{(1)}_{l-1}-h^{(1)}_{l+1}}{h^{(1)}_{l}}\right) j_l - (j_{l-1}-j_{l+1})\right]\Big|_{r_o}} \\
g^{\pm}_{lm}(r_o) &= \frac{1}{h^{(1)}_l\left(\frac{\omega^{\pm}_{m}}{c_s}r_o\right)} - \frac{\left(1\pm 2m\frac{\Omega_o}{\Omega_r}\right) + \frac{\omega^{\pm}_{m}}{c_s}\left(\frac{h^{(1)}_{l-1}-h^{(1)}_{l+1}}{h^{(1)}_{l}}\right)\Big|_{r_o}}{\frac{\omega^{\pm}_{m}v}{2\mathcal{M}}\left[\left(h^{(1)}_{l-1}-h^{(1)}_{l+1}\right) - h^{(1)}_l\left(\frac{j_{l-1}-j_{l+1}}{j_l}\right)\right]\Big|_{r_o}}
\end{aligned}
$$

3.3 Results

We proceed in our analysis by looking at the density wakes formed by perturbers in the subsonic ($\mathcal{M} < 0.8$), transonic ($\mathcal{M} \sim 0.8 - 1.3$), and supersonic regimes ($\mathcal{M} \sim 1.3 - 5.0$). Note that as we increase the velocity of the perturber, we keep the nature of the slightly eccentric orbit that we are studying by keeping the precession frequency, $\Omega_{pr} = \Omega_o - \Omega_r$, constant for all cases. The density profiles presented in this section are on the orbital plane, $\theta = \frac{\pi}{2}$.

3.3.1 Solution matching at the orbital radius

Previously, we were able to match the solutions inside and outside the orbital radius by applying the continuity and jump conditions that we have derived from our wave equation. Presented in Figure 3.2 is a plot of the density perturbation in a fluid with speed of sound $c_s = 0.4$, over r, in the subsonic ($\mathcal{M} = 0.5$), transonic ($\mathcal{M} = 1.3$), and supersonic (relativistic) ($\mathcal{M} = 2.25$) regimes.

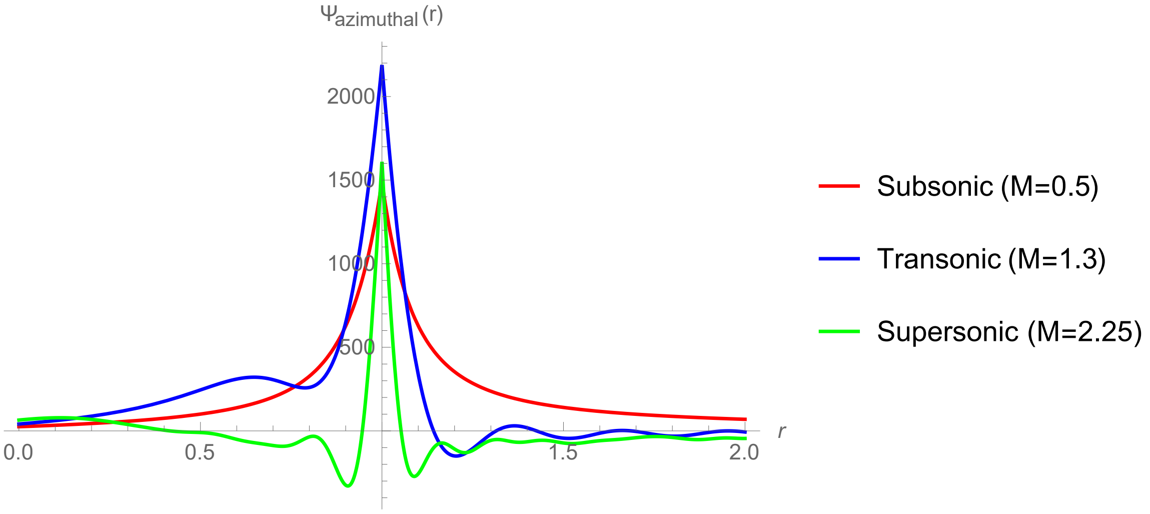

Figure 3.1: Plot of $\Psi^o(r)$ in the subsonic, transonic, and supersonic regimes, within the interval $r \in [0, 2]$, where r is scaled with respect to r_o.

Notice that, for all cases, our implemented jump and continuity conditions hold; that is, for each plot, the function appears to be continuous at the boundary, and the derivatives do not agree. This verifies our claim that we have successfully matched the solutions at the boundary for the main frequency solution.

We can observe that the wavefunction solution for the sidebands is not continuous at the boundary, and the derivatives do not agree with each other. This confirms that

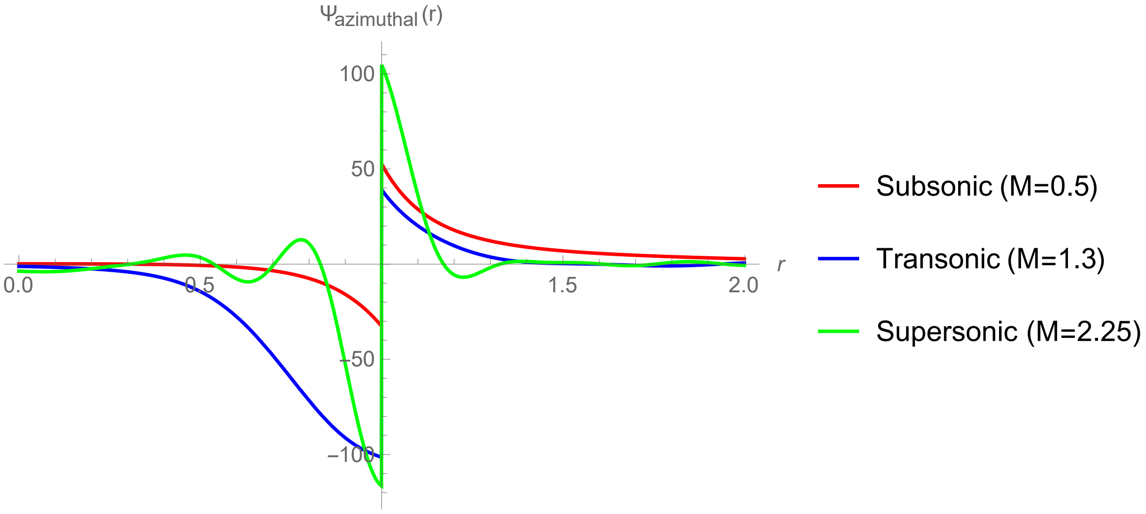

Figure 3.2: Plot of $\chi^{\pm}(r)$ in the subsonic, transonic, and supersonic regimes, within the interval $r \in [0, 2]$, where r is scaled with respect to r_o.

we have implemented our jump conditions correctly.

3.3.2 Numerical cutoff for contributions over l modes

Our solution for the density perturbation induced in the fluid involves a sum over l and m. Numerically summing over l, from 0 to infinity, is impossible but unnecessary, especially when we expect that the sum should converge to a value that is within our desired precision over a certain number of l mode contributions. However, for the mode sum of a smooth function, it is guaranteed that it will converge exponentially for all values of x^i, which is a general property of the multipole expansion [50]. Thus, we expect that each l mode contribution must fall off exponentially.

Shown in Figures 3.3 and 3.4 are discrete plots over each l mode contribution for the density perturbation solutions inside and outside the orbital radius, r_o.

We can easily observe the exponential falloff by looking at Figure 3.3a, and verify this behavior in the logarithmic plot shown in Figure 3.3b. In this study, contributions of order 10^{-2} and below are considered as noise; thus, we can consider a mode sum of only up to 10 l contributions.

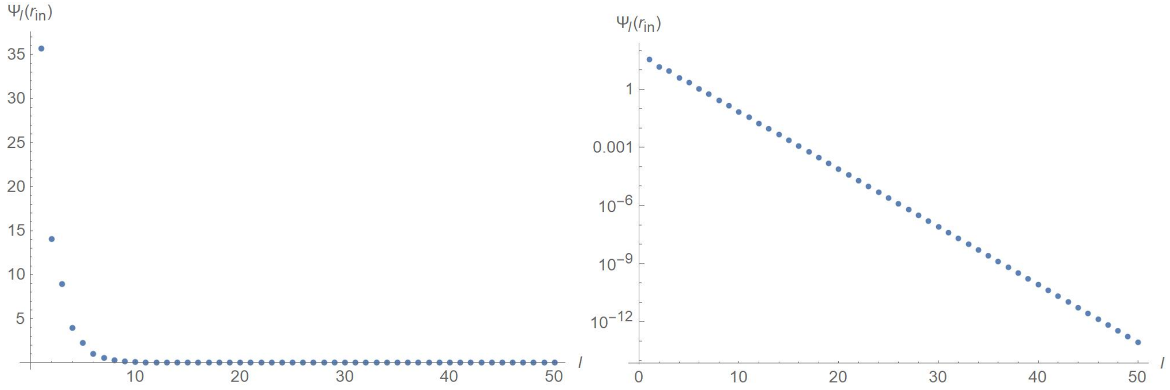

(a) (b)

Figure 3.3: (a) Discrete plot of Ψ_l inside the orbital radius, for each l contribution and (b) the same plot in logarithmic scale

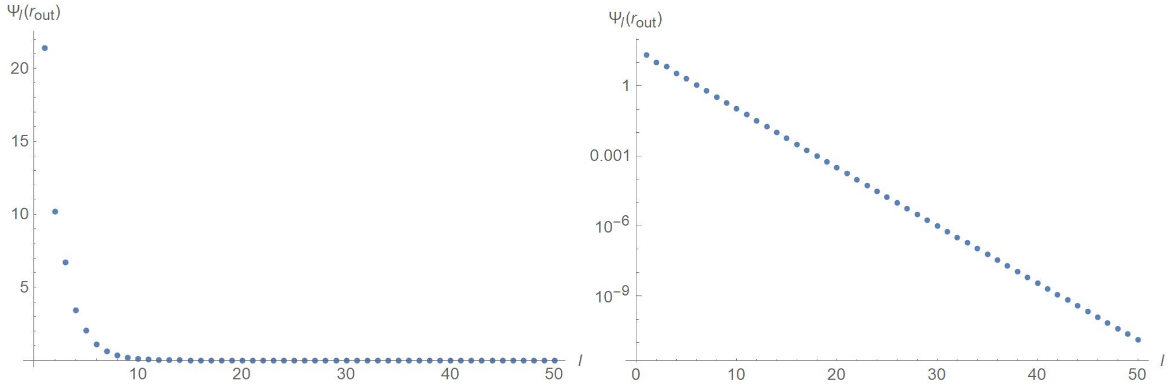

(a) (b)

Figure 3.4: (a) Discrete plot of Ψ_l outside the orbital radius, for each l contribution and (b) the same plot in logarithmic scale

The same logarithmic decay can be observed in Figure 3.4b such that the cutoff that we have previously imposed still requires at least 10 l modes.

3.3.3 Behavior of the density wake

It is important to consider in this analysis that we are already looking at the steady-state behavior of the density wake. This justifies the appearance of a trail for $t = 0$ in the temporal evolution of the density profiles. Also, unlike that of Kim & Kim's [14] method, we did not proceed in solving for the wave equation in the temporal domain, rather in the frequency domain. We argue that this is more efficient and does not need an initial condition to evolve from, which when set may seem unphysical (e.g. turning on the perturbation at some time t, which equivalently means that a massive particle suddenly appears from nowhere.) For all the density profiles presented for each regime, the time t is scaled to $\frac{r_o}{c_s}$.

Subsonic cases ($\mathcal{M} < 0.8$)

Shown in Figure 3.10 are density plots that display the temporal evolution of the density perturbation induced by a moving perturber, with Mach number $\mathcal{M} = 0.5$, through a fluid with speed of sound $c_s = 0.4\ c$. We can see, although faint that the density wake is centered at the perturber for all times, and that it is smoothly distributed throughout. This implies that the perturber is slow enough just for it to travel with the density wake that it induces on the fluid. For this case, however, our visualization seem to correspond to the density profile of a perturber moving at a subsonic speed along a straight-line like that of Ostriker's result [13]. This may imply that the perturber that we are observing is not moving fast enough for its density wake to bend towards its trajectory like that of Kim & Kim's hydrodynamic simulation [14] for the same Mach number. Because of the approximate spherical symmetry of the wake, we expect that both the radial and azimuthal contributions to the DF experienced by the perturber would closely agree with that of the straight-line case for subsonic speeds.

It is possible that this behavior is only a matter of choice in the parameters since our classification depend on what we set our fluid's sound speed to be. In Figures 3.5 and 3.11, we have set $\mathcal{M} = 0.7$ to look into a near-transonic case and observe its density wake. We can see in the figure below that a faint tail that slightly curves toward the perturber's trajectory is already visible. Thus, we can say that indeed, the particle with $\mathcal{M} = 0.5$ is not fast enough to leave a density tail.

Moreover, the wake around the perturber is smoothly distributed, but asymmetric. This corresponds to an unequal DF effect due to the radial and azimuthal directions.

Transonic case ($\mathcal{M} \sim 0.8 - 1.3$)

In the transonic case (Figures 3.12 and 3.13), we can observe a dominant density trail that is sharply defined compared to its background. Notice that unlike the density profiles presented by Kim [14], there is a noticeable set of lesser density trails that are equally spaced about the trail from the perturber, as seen in Figure 3.6.

Although, compared to the main density trail near the perturber, its magnitude is subdominant. Another color scaling may be of use in further defining the density profile, like a logarithmic scale which was used in [14]. However, for our purposes, this color scheme is enough for us to identify the density wake induced by the moving perturber and observe its evolution.

In another case wherein the perturber has a Mach number $\mathcal{M} = 1.3$, whose magnified version is shown above, we can observe that the wake seems to have expanded, while the Mach cone have engulfed the perturber, creating a higher density perturbation near the perturber. We can infer qualitatively from this density profile, that the dynamical friction effect would have been greatest in this case.

Supersonic case ($\mathcal{M} \sim 1.3 - 5.0$)

We proceed in the same manner as the previous cases, and look into two Mach numbers, as shown in Figures 3.14 and 3.15, for the same sound speed $c_s = 0.4\ c$, one of which corresponds to a relativistic speed at 0.9 c. For $\mathcal{M} = 1.8$, the Mach cone seems to have elongated further and the density trail became thicker than in the transonic case. Shown in Figure 3.8a is a density plot with an inset of a magnified image of the plot at the position of the perturber, wherein one can see an abrupt change in the density perturbation around the vicinity of the perturber. The Mach cone is also visibly wider, while the tail is thicker than in the case when $\mathcal{M} = 1.8$.

From this, one can infer that as we increase the Mach number of the perturber from unity, the density tail thickens as well. We expect that for a simulation that incorporates a higher resolution we can see the interaction of the other point (as pointed by a gray block arrow in Figure 3.8a) at the tip of the Mach cone which we have unidentified, and the perturber for increasing values of the Mach number.

3.3.4 Sideband contributions

Presented in Figure 3.9 are density plots of the sideband contributions that we have previously evaluated. One can easily notice that these density plots exhibit the same behavior as the density plots of each case that they represent. However, the magnitudes presented in their color scale signal that the perturbation that we have introduced to the system has a subdominant effect on the physical system that we have considered.

3.3.5 Summary

Through these observations, we confirm that induced density perturbations in the relativistic regime behave quite similarly to those in the Newtonian regime. Moreover, we see subdominant density trails that are equally spaced from the density trail behind the perturber's trajectory. There are no noticeable density trails other than the one following the perturber's trajectory in the subsonic and supersonic regime.

We use the expressions that we obtained in deriving expressions for the metric perturbations induced in our perturbed flat spacetime background, which, in turn, serves as a preliminary step to fully solving for the dynamical friction effects for slightly-eccentric orbits.

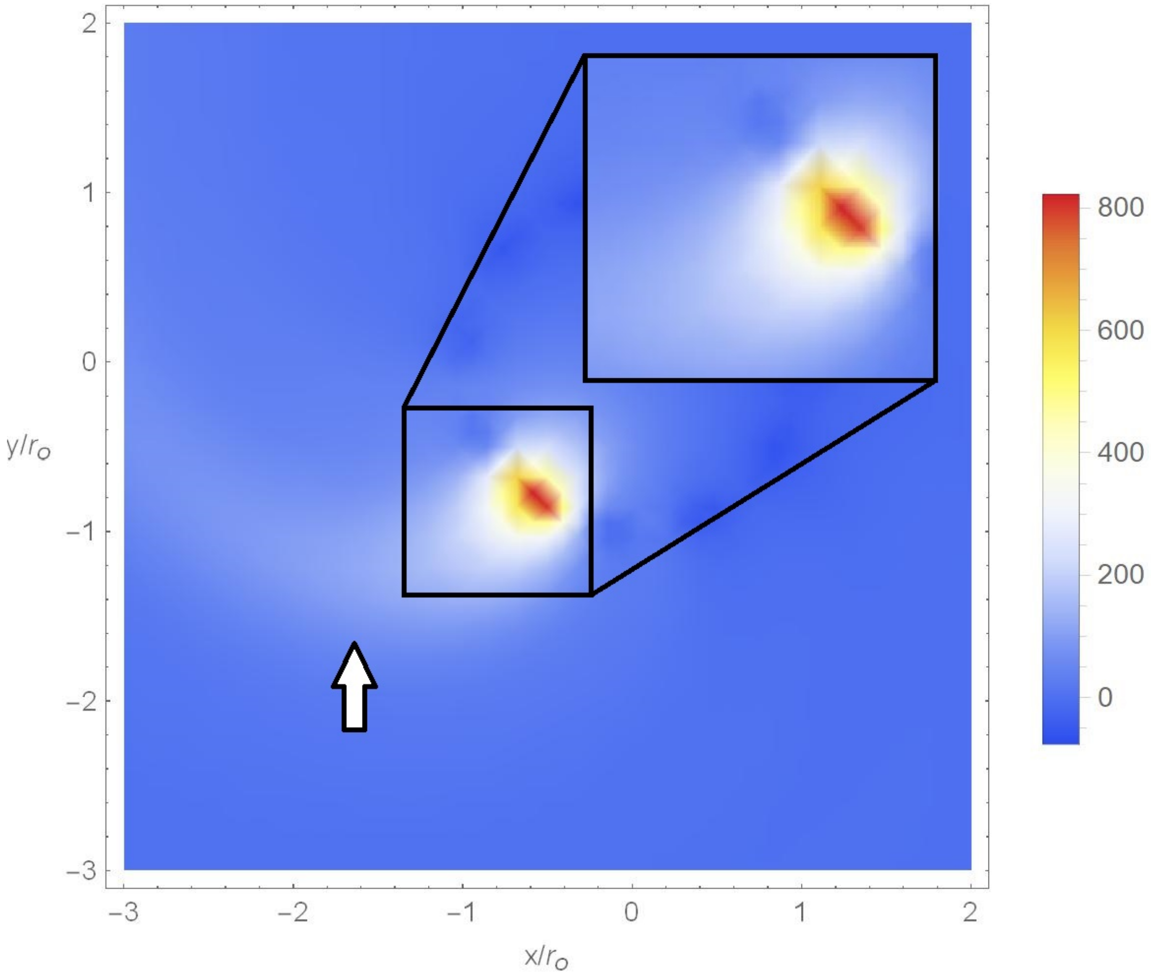

Figure 3.5: Density plot of a perturber moving with Mach number,$\mathcal{M} = 0.7$. The white block arrow points at the faint density trail formed by a perturber moving at a near-transonic speed. The magnified inset of the plot at the position of the perturber reveals a smoothly distributed overdensity around it.

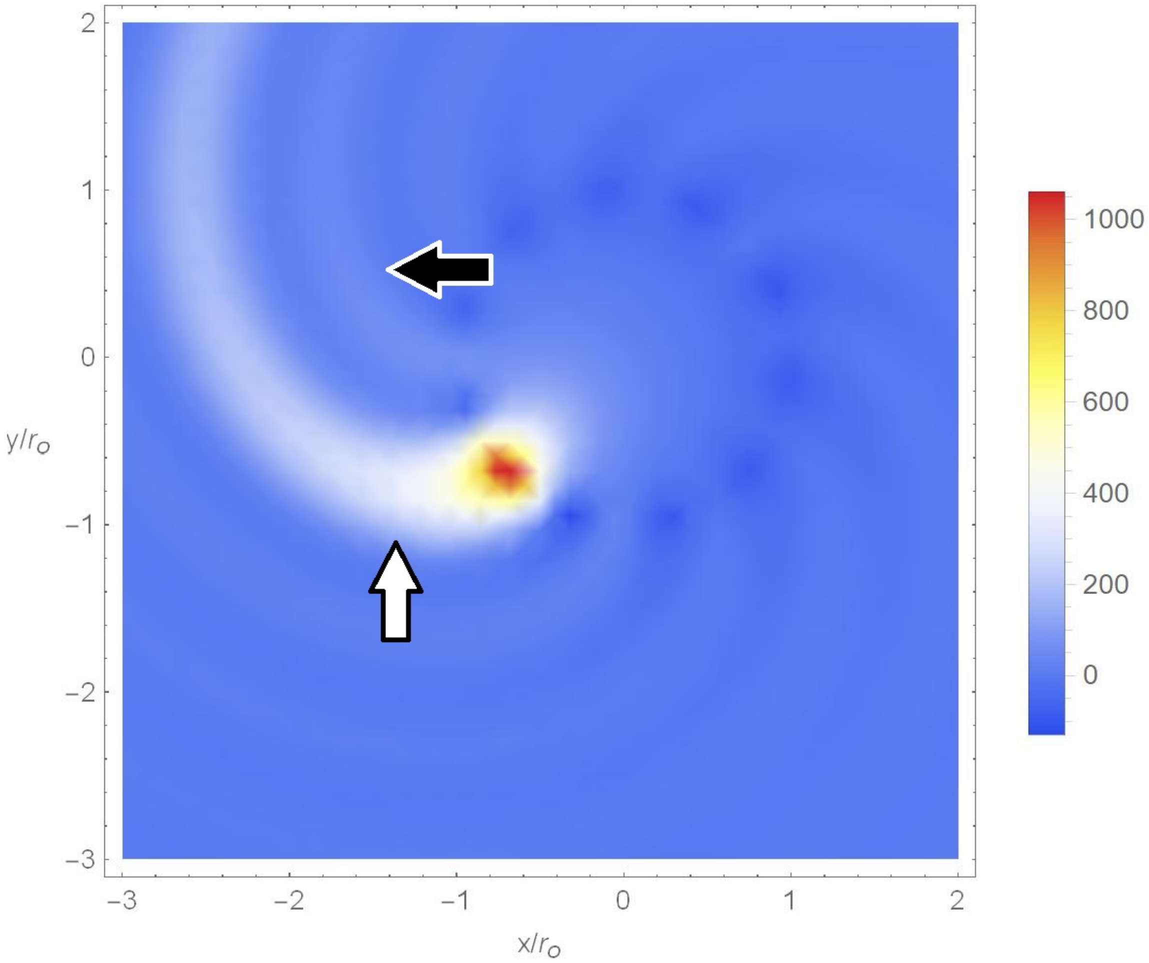

Figure 3.6: Density plot for a perturber with Mach number $\mathcal{M} = 0.9$. We can already notice a long density trail, pointed by a white block arrow, following the perturber's trajectory, which was already observed in simulations of black hole mergers in gaseous media by Refs [51, 52, 53]. Lesser density trails (pointed by a black block arrow) are also visible near the perturber. However, its magnitude decreases as we consider points farther away from the perturber.

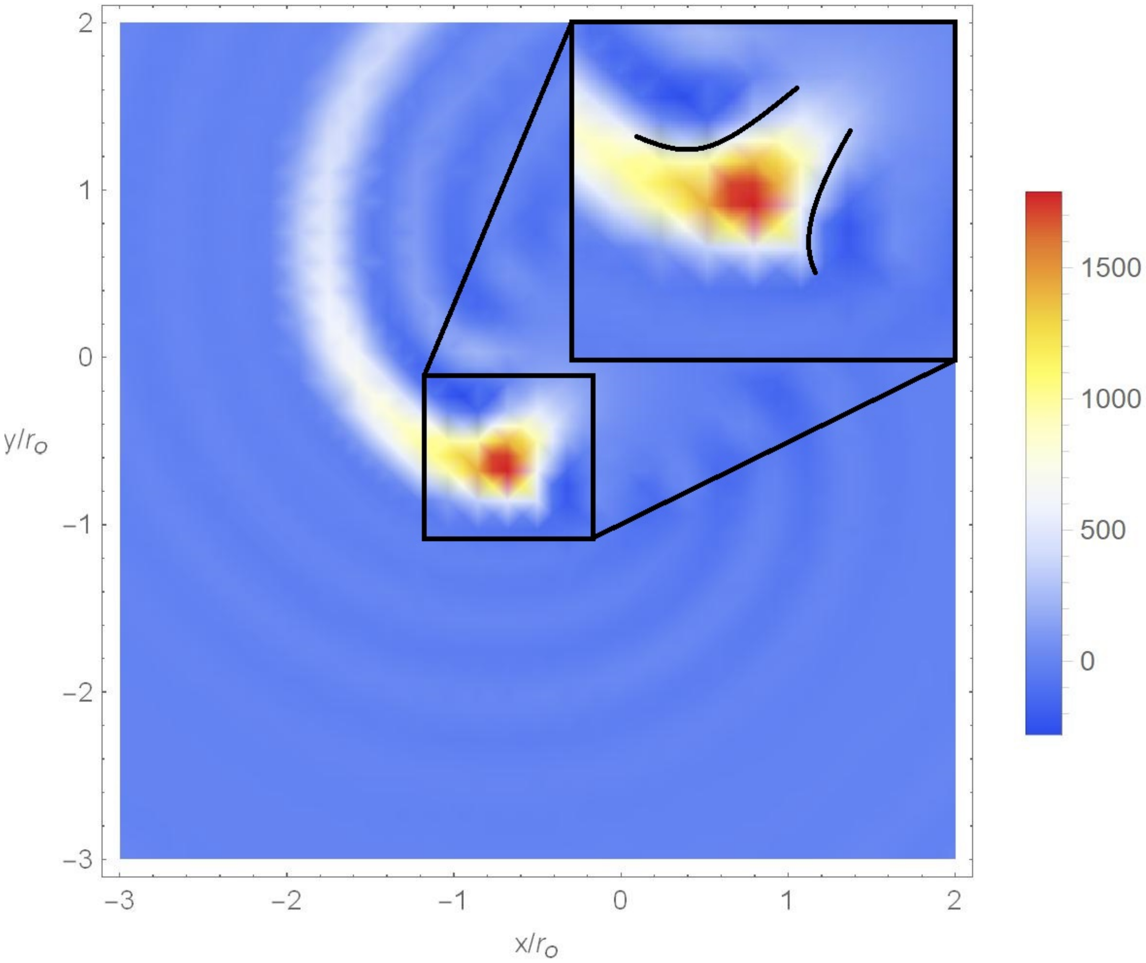

Figure 3.7: Density plot for a perturber moving at a near-supersonic speed. There is a visible formation of the Mach cone, likewise curved towards the trajectory, that engulfs the perturber, thereby increasing the magnitude of the overdensities in the vicinity, for $\mathcal{M} = 1.3$

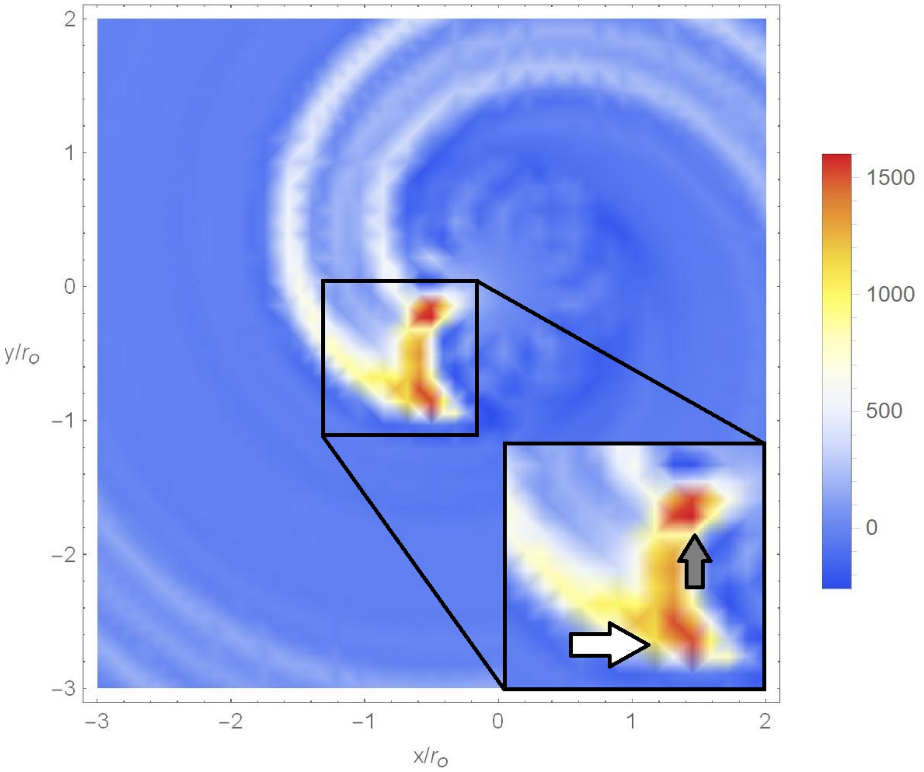

(a)

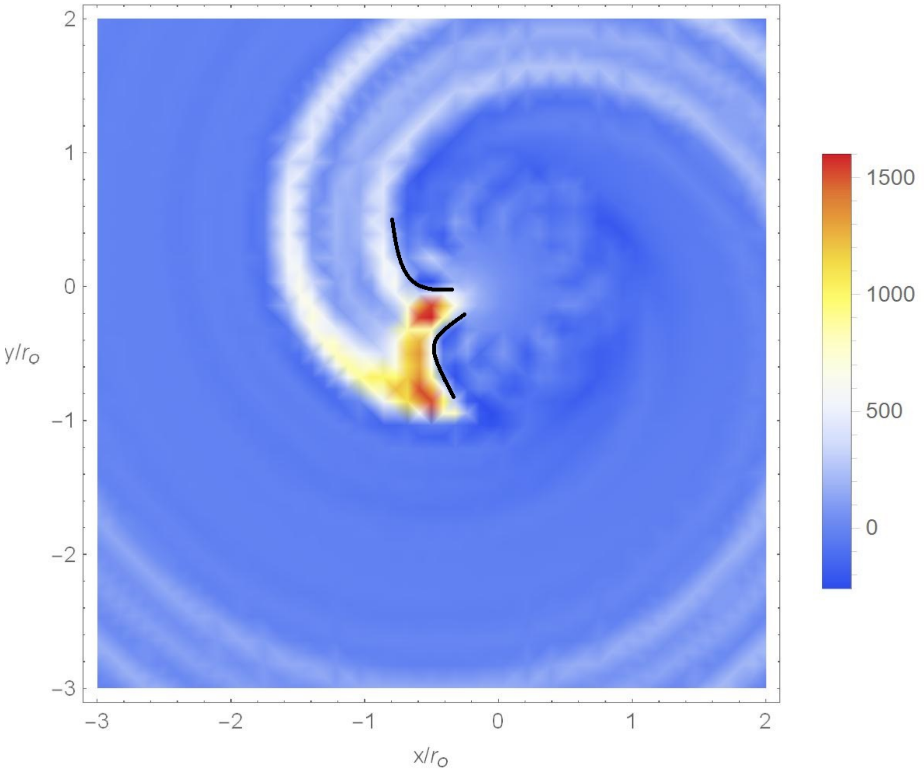

(b)

Figure 3.8: (a) The perturber (pointed by a white block arrow) has already overtaken its Mach cone, thereby creating a shock which is signalled by the abrupt change in density perturbation around its vicinity. (b) Also, the Mach cone is considerably wider than that of the transonic case

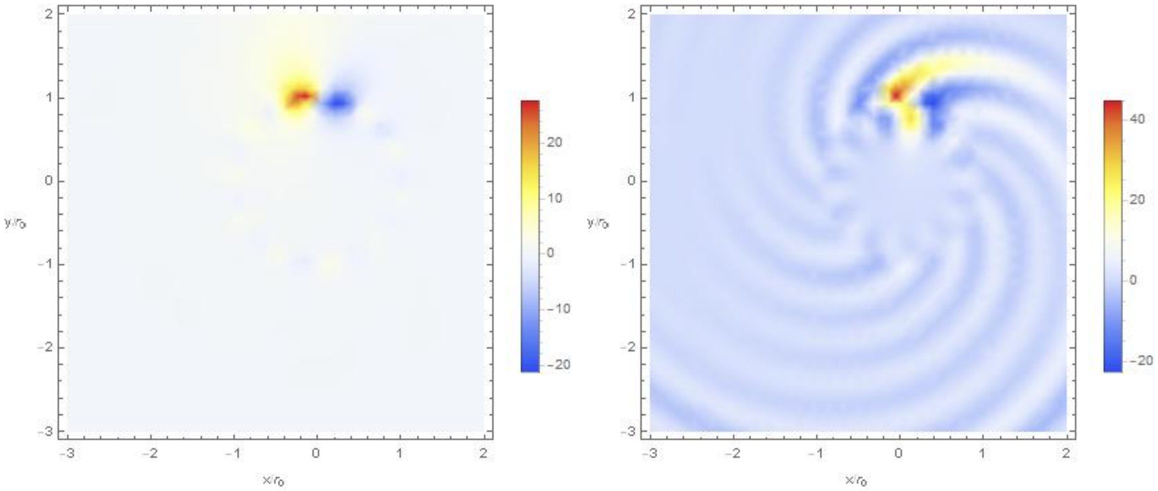

(a) Subsonic (b) Transonic

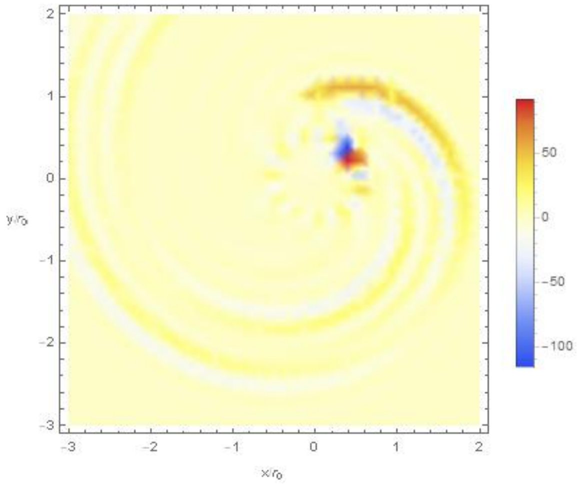

(c) Supersonic

Figure 3.9: Density plots of the sideband solutions for (a) subsonic, (b) supersonic, and (c) supersonic cases. The behavior of the sideband contribution's density plots are the same as that of the whole solution; however, one must notice that the magnitudes in their color scale are much less than that of the presented plots earlier. Therefore, we can say that the perturbations that we have introduced have a subdominant effect compared to the main frequency contribution that represents the circular orbit case (i.e. $\delta R = 0$).

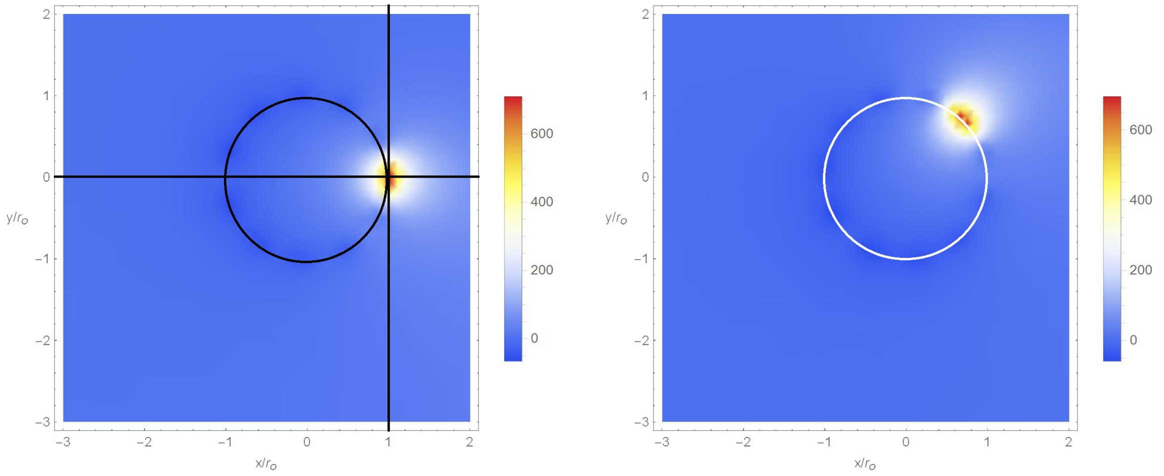

(a) $t(r_o/c_s) = 0$ (b) $t(r_o/c_s) = 0.79$

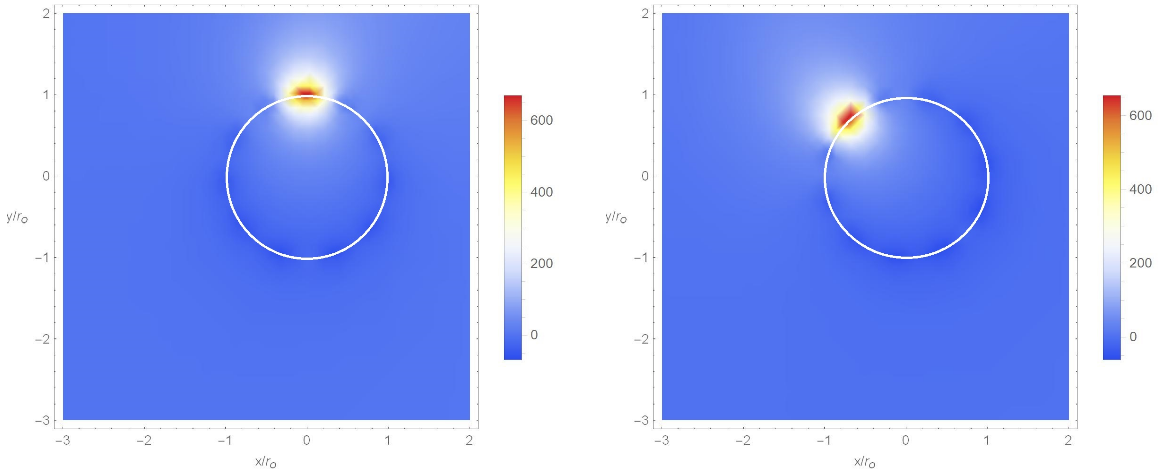

(c) $t(r_o/c_s) = 1.57$ (d) $t(r_o/c_s) = 2.37$

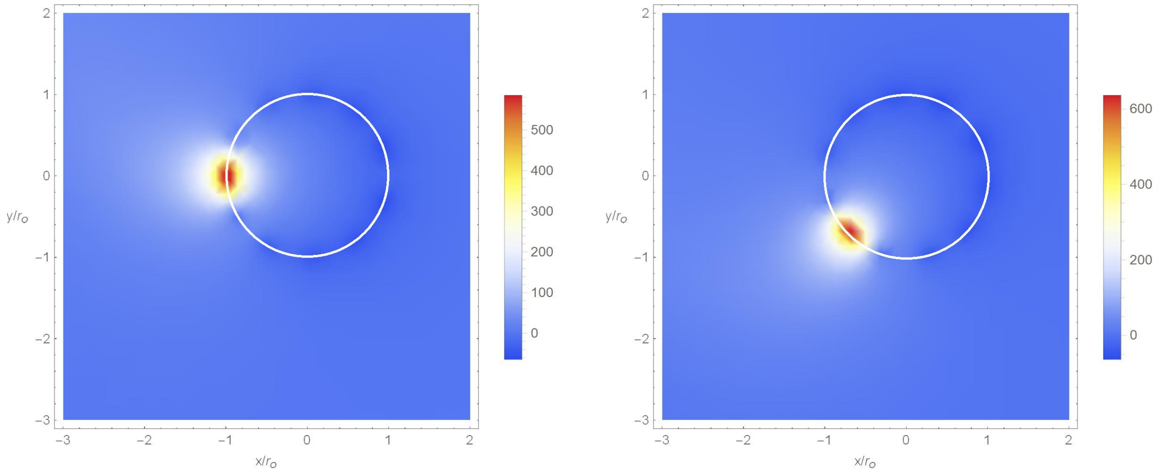

(e) $t(r_o/c_s) = 3.14$ (f) $t(r_o/c_s) = 3.92$

Figure 3.10: Temporal evolution of density perturbations in the subsonic case ($\mathcal{M} = 0.5$). The density wake is smoothly distributed around the perturber for all time slices, which corresponds to the straight-line case by Ostriker [13] for subsonic speeds. In all time slices, we define t in units of $\frac{r_o}{c_s}$. White circles represent the circular orbit that the test particle follows.

.

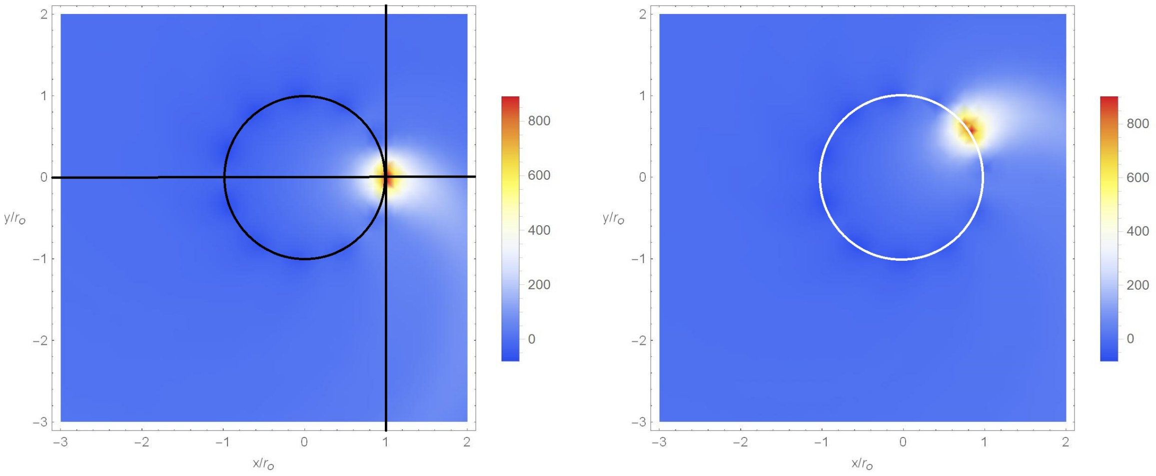

(a) $t(r_o/c_s) = 0$ (b) $t(r_o/c_s) = 0.79$

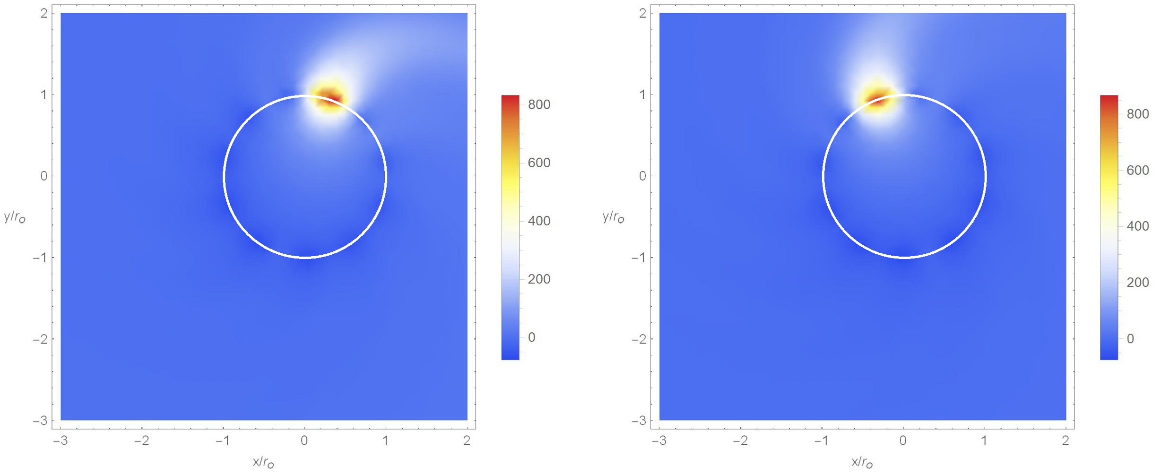

(c) $t(r_o/c_s) = 1.57$ (d) $t(r_o/c_s) = 2.37$

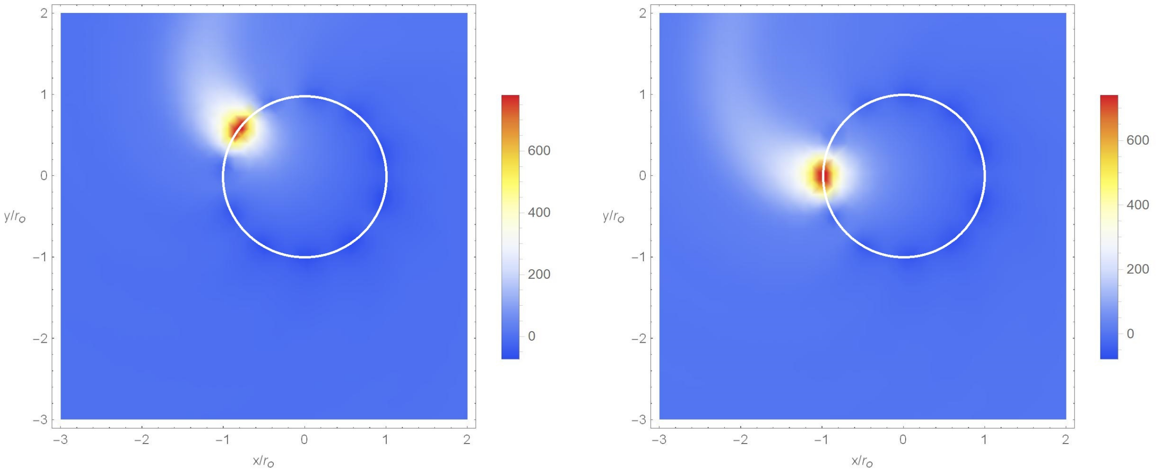

(e) $t(r_o/c_s) = 3.14$ (f) $t(r_o/c_s) = 3.92$

Figure 3.11: Temporal evolution of density perturbations in the subsonic case ($\mathcal{M} = 0.7$). We can already observe a faint density trail behind the trajectory of the perturber, which curves toward its trajectory. In all time slices, we define t in units of $\frac{r_o}{c_s}$.White circles represent the circular orbit that the test particle follows.

.

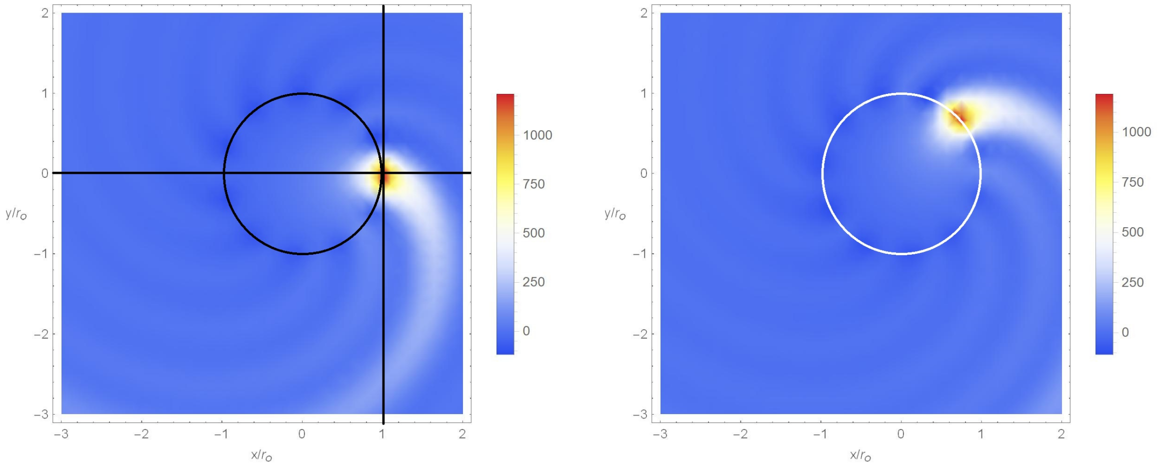

(a) $t(r_o/c_s) = 0$ (b) $t(r_o/c_s) = 0.79$

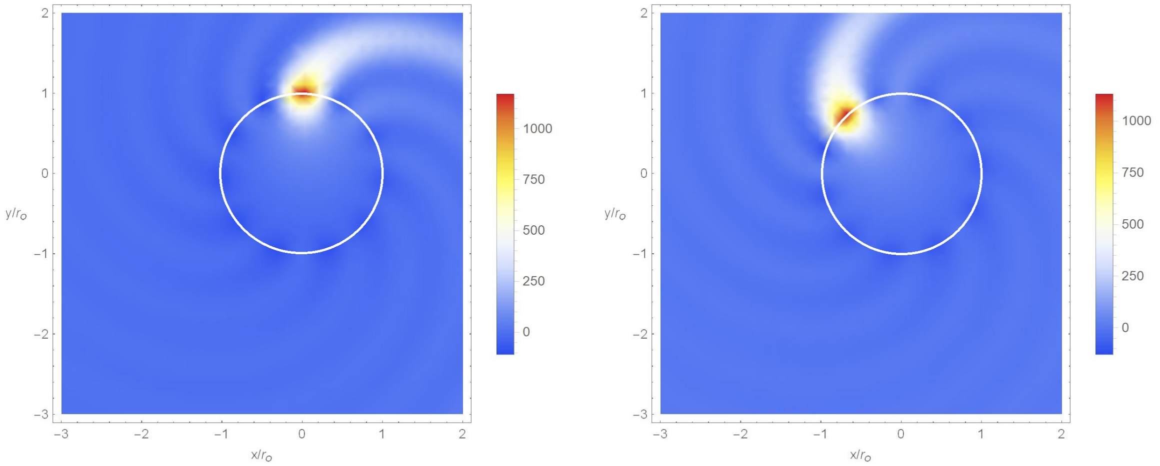

(c) $t(r_o/c_s) = 1.57$ (d) $t(r_o/c_s) = 2.37$

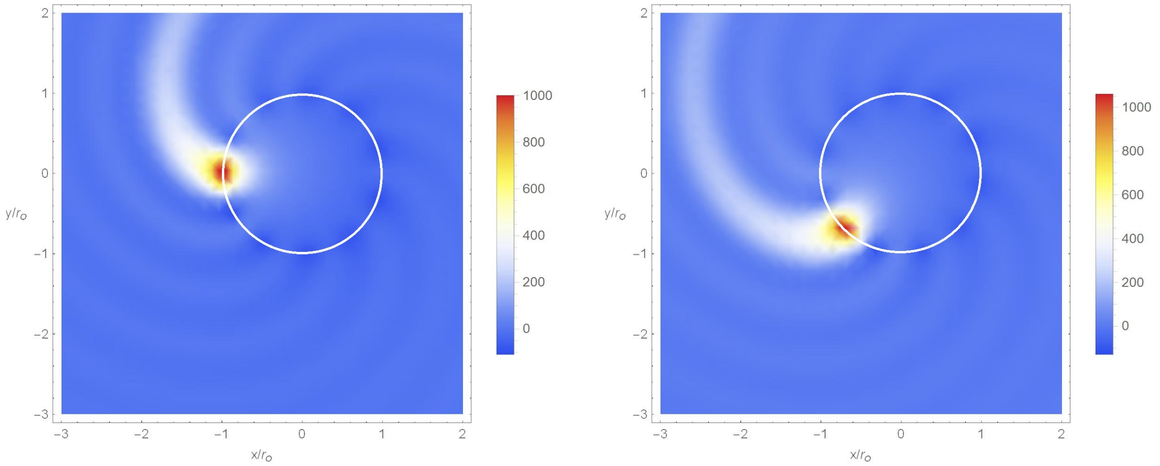

(e) $t(r_o/c_s) = 3.14$ (f) $t(r_o/c_s) = 3.92$

Figure 3.12: Temporal evolution of density perturbations in the transonic case ($\mathcal{M} = 0.9$). We can already see a density trail with a structure distinct from the ambient environment of the perturber. Also, lesser density trails are already visible in this case. White circles represent the circular orbit that the test particle follows.

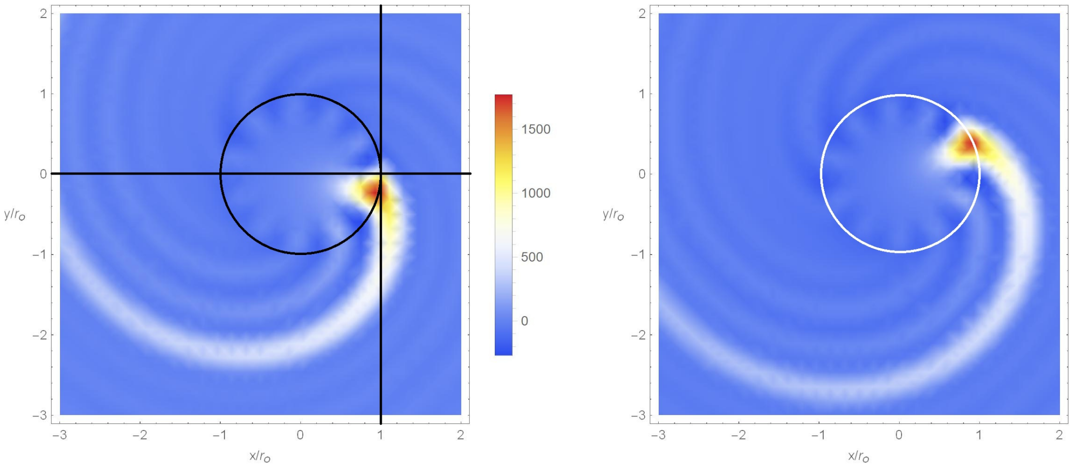

(a) $t(r_o/c_s) = 0$ (b) $t(r_o/c_s) = 0.79$

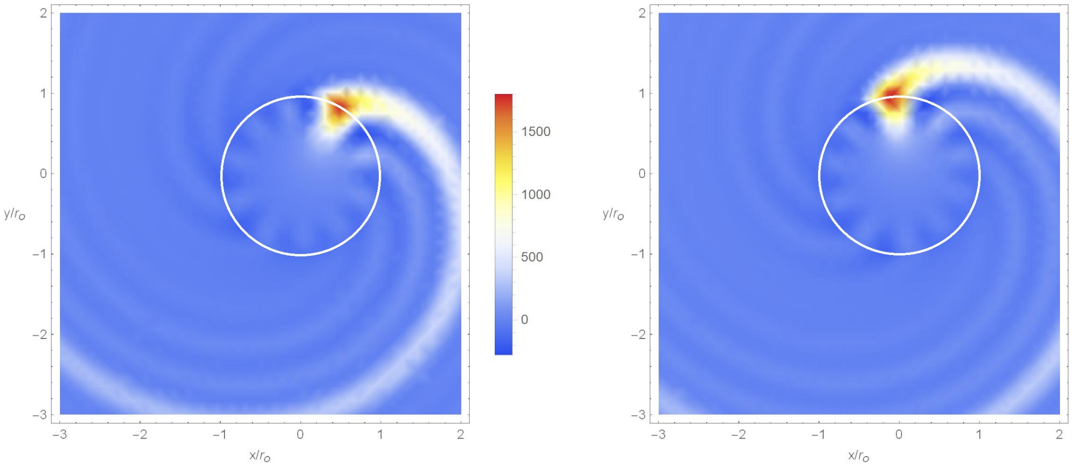

(c) $t(r_o/c_s) = 1.57$ (d) $t(r_o/c_s) = 2.37$

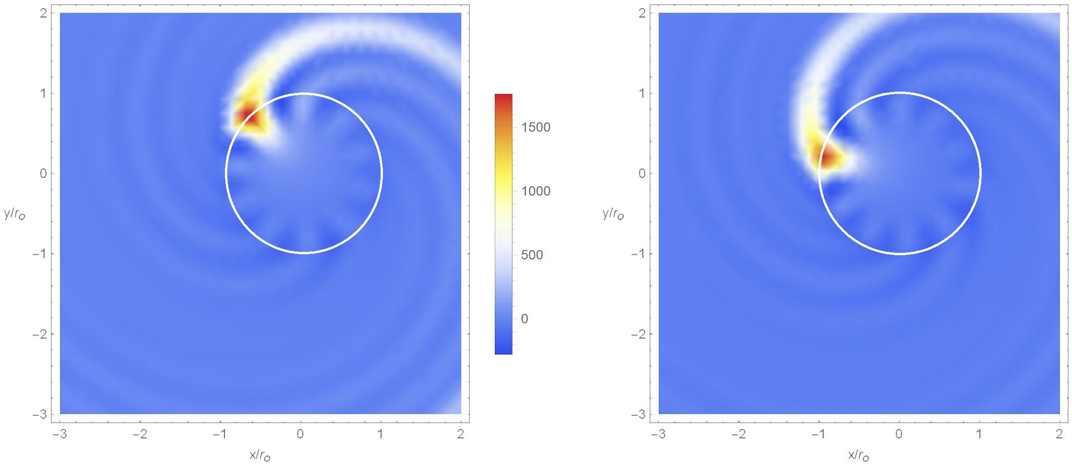

(e) $t(r_o/c_s) = 3.14$ (f) $t(r_o/c_s) = 3.92$

Figure 3.13: Temporal evolution of density perturbations in the transonic case ($\mathcal{M} = 1.3$). The formation of a conic structure (that is, the Mach cone) engulfs the perturber which might have induced the twofold increase in magnitude compared to the perturbations in the subsonic case. White circles represent the circular orbit that the test particle follows.

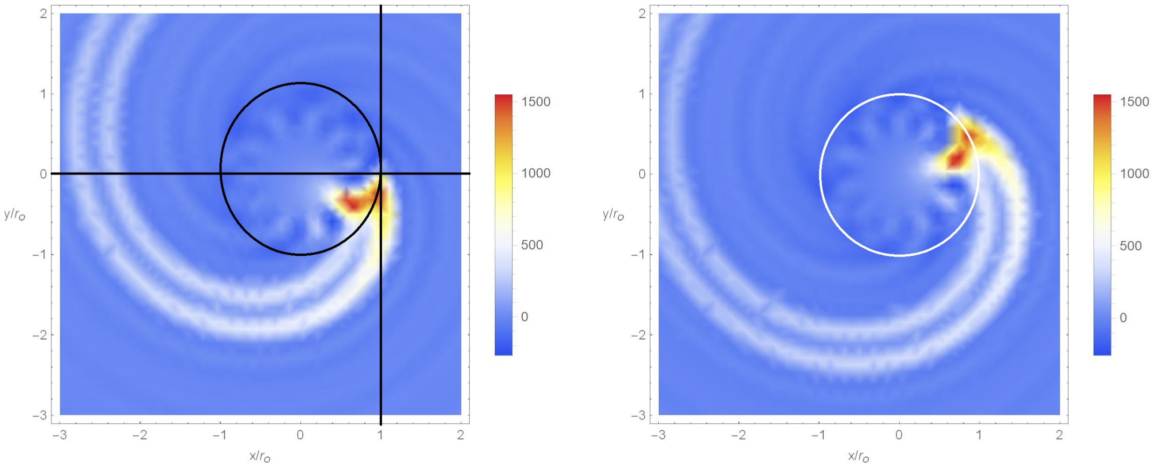

(a) $t(r_o/c_s) = 0$

(b) $t(r_o/c_s) = 0.79$

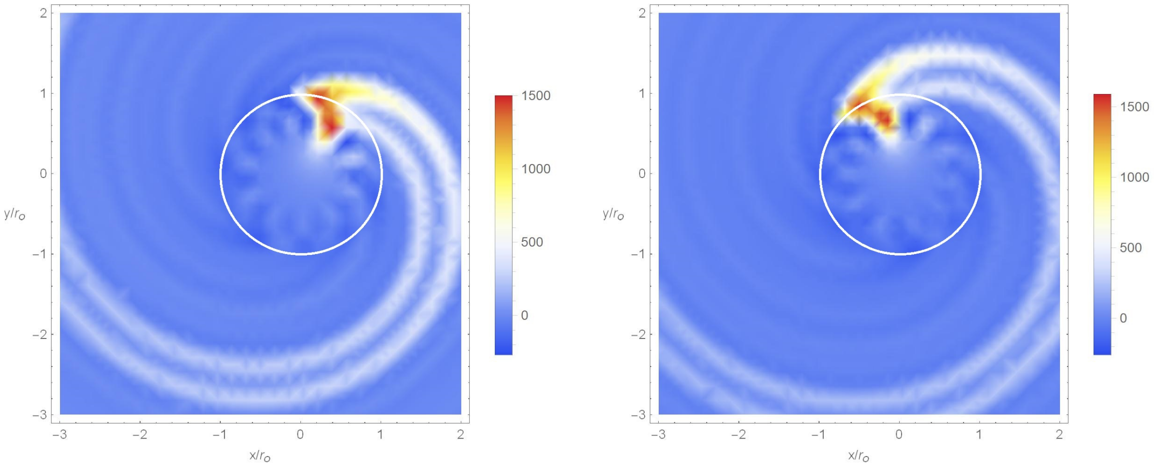

(c) $t(r_o/c_s) = 1.57$

(d) $t(r_o/c_s) = 2.37$

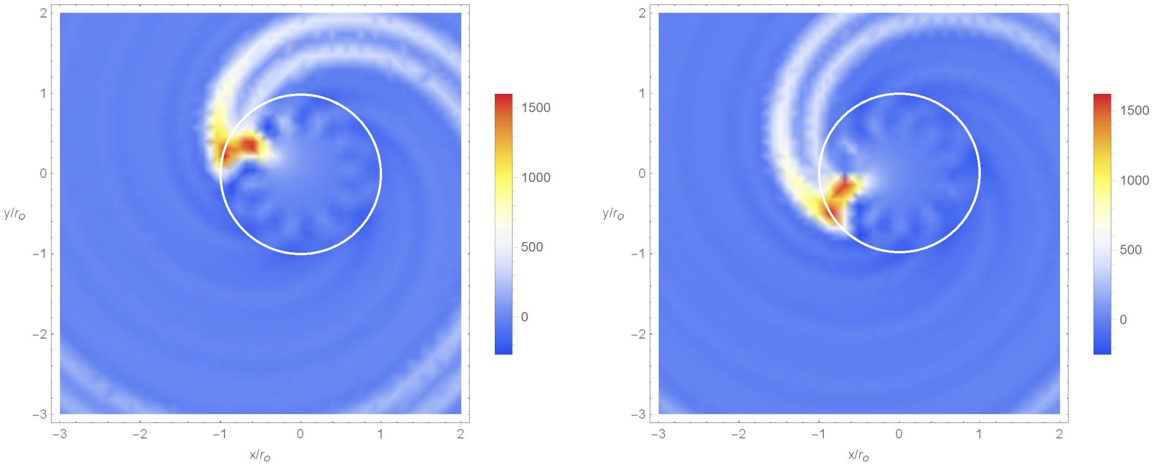

(e) $t(r_o/c_s) = 3.14$

(f) $t(r_o/c_s) = 3.92$

Figure 3.14: Temporal evolution of density perturbations in the supersonic case ($\mathcal{M} = 1.8$). In this case, the perturber has already overtaken its Mach cone producing a shock front that serves as a boundary between the region inside the density trail behind the perturber and its ambient environment. One can also notice that the Mach cone is wider than in the transonic case. White circles represent the circular orbit that the test particle follows.

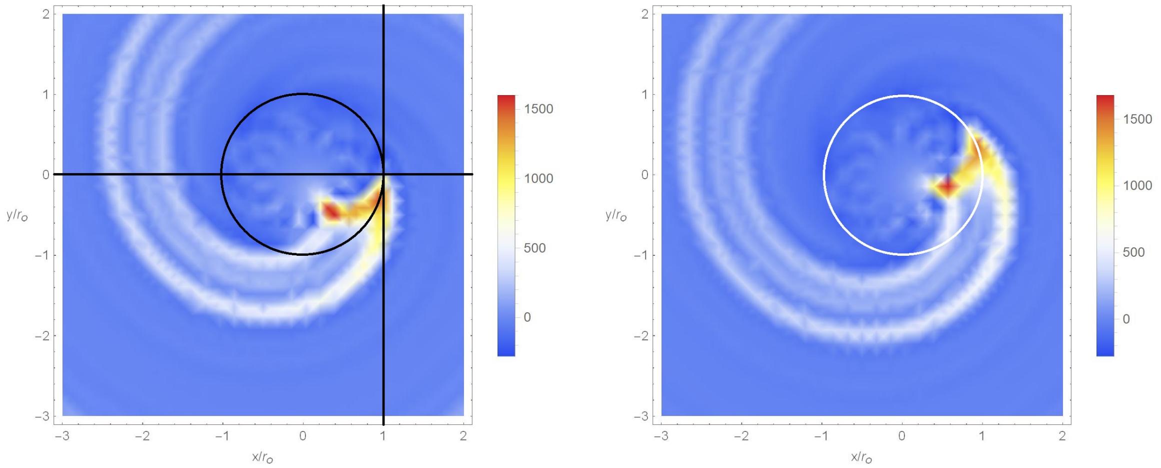

(a) $t(r_o/c_s) = 0$ (b) $t(r_o/c_s) = 0.79$

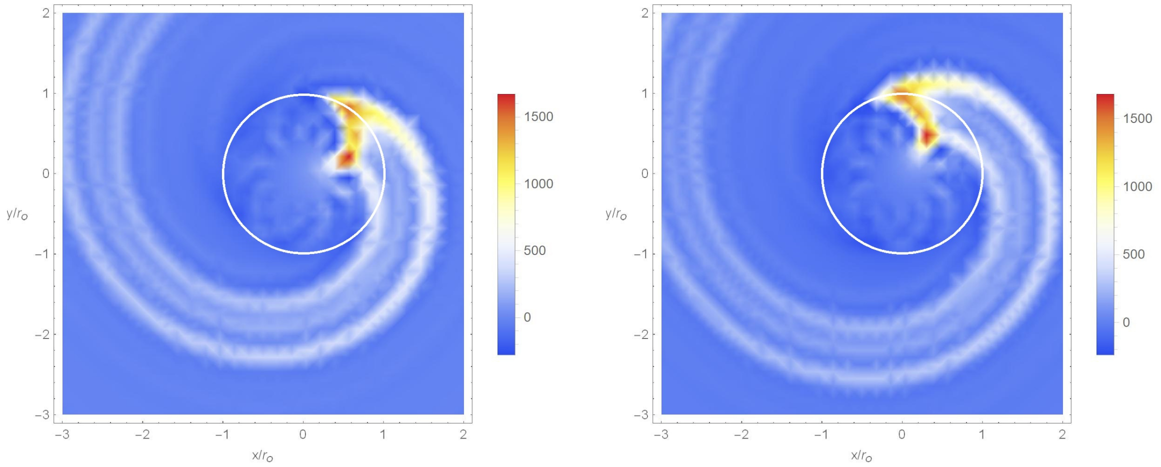

(c) $t(r_o/c_s) = 1.57$ (d) $t(r_o/c_s) = 2.37$

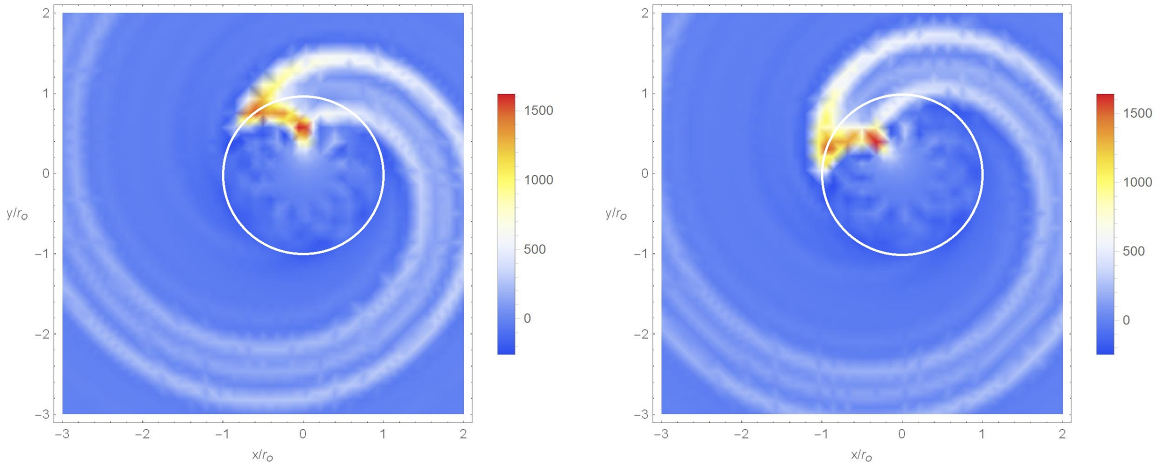

(e) $t(r_o/c_s) = 3.14$ (f) $t(r_o/c_s) = 3.92$

Figure 3.15: Temporal evolution of density perturbations in the supersonic case ($\mathcal{M} = 2.25$). Compared to a perturber moving with Mach number $\mathcal{M} = 1.8$, the tail and Mach cone in this case are wider. White circles represent the circular orbit that the test particle follows.

3.4 Metric perturbation gradients

The expression for the metric perturbations induced in the fluid due to presence of the perturber,ψ^{fluid}, is given by Equation (2.33). We present it again in this subsection to serve as an easy reference for the proceeding calculations.

$$\partial_i\psi^{\text{fluid}}(\mathbf{x},t) = -(\rho+p)\int d^3x'\frac{\delta n}{n}(\mathbf{x}',t)\frac{(\mathbf{x}-\mathbf{x}')\cdot\partial_i\mathbf{x}}{|\mathbf{x}-\mathbf{x}'|^3} \times (1+\varepsilon_{\text{Yukawa}})+\varepsilon_{\text{notDF}} \quad (3.29)$$

Recall that the metric perturbation consists of a part that does not correspond to dynamical friction, ε_{notDF}, and the former expression which is induced by the presence of the overdensities. We rewrite the previous expression in terms of the weight function $\mathcal{W}(\mathbf{x}',t)$, to yield

$$\partial_i\psi^{\text{fluid}}(\mathbf{x},t) = \partial_i\phi^{\text{fluid}} = \frac{4\pi M\gamma(\rho+p)(1+v^2)}{v^2}I_i+\varepsilon_{\text{notDF}}.$$

where,

$$I_i = \mathcal{M}^2\int d^3x'\mathcal{W}(\mathbf{x}',t)\frac{(\mathbf{x}-\mathbf{x}')\cdot\partial_i\mathbf{x}}{|\mathbf{x}-\mathbf{x}'|^3}\times\left(1+\mathcal{O}\left(\frac{\mathcal{L}}{\lambda_J}\right)\right) \quad (3.30)$$

which we evaluate for each coordinate. The complete form of the weight function $\mathcal{W}(\mathbf{x}',t)$ is presented in Appendix A. Note that the weight function is composed of the unperturbed part due to the orbital frequency ω_m^o, $\mathcal{W}_o(\mathbf{x}',t)$, and the perturbation terms composed of the contributions due to the frequency sidebands, $\mathcal{W}_\pm(\mathbf{x}',t)$.

One of our main goals is to develop the δR corrections to the metric perturbation gradients of Ref [16] for ready use in a future work on the full calculation of DF. Note that the system has a symmetry in θ, which implies that all contributions due to θ vanishes completely.

We define $\mathbf{x}$ to be the position vector defining the slightly-eccentric trajectory of the pertuber, such that

$$\mathbf{x} = R(t)\cos\Phi(t)\hat{x}+R\sin\Phi(t)\hat{y} \quad (3.31)$$

and $\mathbf{x}'$ to be the position vector defining any field point in space,

$$\mathbf{x}' = r'\sin\theta'\cos\phi'\hat{x}+r'\sin\theta'\sin\phi'\hat{y}+r'\cos\theta'\hat{z} \quad (3.32)$$

We proceed by expanding our integral in terms of δR up to the linear order, for each coordinate contribution. The magnitude of the separation vector $(\mathbf{x}-\mathbf{x}')$,

$$\frac{1}{|\mathbf{x}-\mathbf{x}'|} = (R(t)^2+r'^2-2R(t)r'\cos(\Phi(t)-\phi')\sin\theta')^{-\frac{1}{2}}$$

which we expand in δR by substituting Equation (3.2) and Equation (3.3) to the previous expression, while keeping only terms of linear order in δR

$$\begin{aligned}\frac{1}{|\mathbf{x}-\mathbf{x}'|} &= \{(r_o+\delta R\cos(\Omega_r t))^2 + r'^2 \\ &\qquad - 2(r_o+\delta R\cos(\Omega_r t))r'\sin\theta'\cos(\Omega_o t-\phi'+\alpha)\}^{-\frac{1}{2}} \\ &= \Big\{r_o^2 + 2\delta R r_o\cos(\Omega_r t) + r'^2 \\ &\qquad - (2r_o r'\sin\theta' + 2r'\delta R\sin\theta'\cos(\Omega_r t)) \\ &\qquad [\cos(\Omega_o t-\phi')\cos(\alpha) - \sin(\Omega_o t-\phi')\sin(\alpha)]\Big\}^{-\frac{1}{2}}\end{aligned}$$

where $\alpha = -\frac{2\delta R}{r_o}\frac{\Omega_o}{\Omega_r}\sin(\Omega_r t)$. Since $\alpha \ll 1$, we can invoke a small angle approximation, such that $\cos(\alpha)\approx 1$ and $\sin(\alpha)\approx\alpha$, giving us

$$\begin{aligned}\frac{1}{|\mathbf{x}-\mathbf{x}'|} &= \Big\{r_o^2 + 2\delta R r_o\cos(\Omega_r t) + r'^2 \\ &\qquad - (2r_o r'\sin\theta' + 2r'\delta R\sin\theta'\cos(\Omega_r t)) \\ &\qquad [\cos(\Omega_o t-\phi') - \alpha\sin(\Omega_o t-\phi')]\Big\}^{-\frac{1}{2}} \\ &= \Big\{r_o^2 + 2\delta R r_o\cos(\Omega_r t) + r'^2 \\ &\qquad - \sin\theta'(2r_o r'\cos(\Omega_o t-\phi') + 2r_o r'\alpha\sin(\Omega_o t-\phi') \\ &\qquad + 2r'\delta R\cos(\Omega_r t)\cos(\Omega_o t-\phi'))\Big\}^{-\frac{1}{2}}\end{aligned}$$

$$\begin{aligned}\frac{1}{|\mathbf{x}-\mathbf{x}'|} &= \Big\{r_o^2 + r'^2 - 2r_o r'\sin\theta'\cos(\Omega_o t-\phi') \\ &\qquad + 2\delta R r_o\cos(\Omega_r t) - \sin\theta'[2r_o r'\alpha\sin(\Omega_o t-\phi') \\ &\qquad + 2r'\delta R\cos(\Omega_r t)\cos(\Omega_o t-\phi')]\Big\}^{-\frac{1}{2}}\end{aligned} \tag{3.33}$$

which effectively reveals the perturbation in linear order of δR. Since $\delta R \ll 1$, we can apply the binomial approximation $(1+x)^\alpha \approx (1+\alpha x)$, which yields the unperturbed expression plus contributions due to δR,

$$\begin{aligned}\frac{1}{|\mathbf{x}-\mathbf{x}'|} &\approx [r_o^2 + r'^2 - 2r_o r'\sin\theta'\cos(\Omega_o t-\phi')]^{-\frac{1}{2}} \\ &\qquad \left\{1 - \delta R\frac{X(t,r',\theta',\phi')}{r_o^2 + r'^2 - 2r_o r'\sin\theta'\cos(\Omega_o t-\phi')}\right\}\end{aligned} \tag{3.34}$$

where

$$X(t,r',\theta',\phi') = r_o\cos(\Omega_r t) + \sin\theta'[2r'\frac{\Omega_o}{\Omega_r}\sin(\Omega_r t)\sin(\Omega_o t-\phi') \\ - r'\cos(\Omega_r t)\cos(\Omega_o t-\phi')] \tag{3.35}$$

which implies that,

$$\frac{1}{|\mathbf{x}-\mathbf{x}'|^3} \approx [r_o^2 + r'^2 - 2r_o r'\sin\theta'\cos(\Omega_o t-\phi')]^{-\frac{3}{2}} \\ \left\{1 - 3\delta R\frac{X(t,r',\theta',\phi')}{r_o^2+r'^2-2r_o r'\sin\theta'\cos(\Omega_o t-\phi')}\right\} \tag{3.36}$$

We turn our attention to the metric perturbations due to each coordinate, and attempt to the same expansion in δR. The same methods done for the expansion magnitude of the separation vector are applied for the proceeding calculations.

3.4.1 Metric perturbations in t

The projection of the separation vector on the time derivative of the perturber's position vector is given by,

$$(\mathbf{x}-\mathbf{x}')\cdot\partial_t\mathbf{x} = -\Omega_r(\delta R)\sin(\Omega_r t)[R(t) - r'\sin\theta'\cos(\Phi(t)-\phi')] \tag{3.37} \\ + \Omega_\phi R(t) r'\sin(\theta')\sin(\Phi(t)-\phi')$$

We expand this expression by substituting our definitions of $R(t)$ and $\Phi(t)$, and keeping all terms with δR in linear order,

$$\begin{aligned}(\mathbf{x}-\mathbf{x}')\cdot\partial_t\mathbf{x} &= -\Omega_r(\delta R)\sin(\Omega_r t)[r_o + \delta R\cos(\Omega_r t) - r'\sin\theta'\cos(\Omega_o t-\phi'+\alpha)] \\ &\quad + \Omega_\phi(r_o+\delta R\cos(\Omega_r t))r'\sin\theta'\sin(\Omega_o t-\phi'+\alpha) \\ &= -\Omega_r(\delta R)\sin(\Omega_r t)\{r_o + \delta R\cos(\Omega_r t) - \\ &\qquad r'\sin\theta'[\cos(\Omega_o t-\phi')\cos(\alpha) - \sin(\Omega_o t-\phi')\sin(\alpha)]\} \\ &\quad + \Omega_o\left(1 - \frac{2\delta R}{r_o}\cos(\Omega_r t)\right)(r_o+\delta R\cos(\Omega_r t)) \\ &\qquad r'\sin\theta'[\sin(\Omega_o t-\phi')\cos(\alpha) + \cos(\Omega_o t-\phi')\sin(\alpha)] \\ &= -\Omega_r r_o(\delta R)\sin(\Omega_r t) \\ &\quad + \Omega_r(\delta R)\sin(\Omega_r t)r'\sin\theta'\cos(\Omega_o t-\phi') \\ &\quad - \Omega_o r'(\delta R)\cos(\Omega_r t)\sin\theta'\sin(\Omega_o t-\phi') \\ &\quad - 2(\delta R)\frac{\Omega_o^2}{\Omega_r}r'\sin\theta'\cos(\Omega_r t)\cos(\Omega_o t-\phi') \\ &\quad + \Omega_o r' r_o\sin\theta'\sin(\Omega_o t-\phi')\end{aligned}$$

which yields,

$$\begin{aligned}(\mathbf{x}-\mathbf{x}')\cdot\partial_t\mathbf{x} = \Omega_o r' r_o \sin\theta' \sin(\Omega_o t-\phi')+ \\ \delta R\Big\{ r'\sin\theta' \Big[\Big(\frac{\Omega_r - 2\Omega_o^2}{\Omega_r}\Big)\sin(\Omega_r t)\cos(\Omega_r t-\phi') \\ - \Omega_o\cos(\Omega_r t)\sin(\Omega_o t-\phi')\Big] - \Omega_r r_o \sin(\Omega_r t)\Big\}\end{aligned} \tag{3.38}$$

Substituting this expression back to Equation (3.30) gives us an expansion in δR due to the small eccentricity of the orbit,

$$\begin{aligned} I_t &= \mathcal{M}^2\int d^3x'\,[\mathcal{W}_o(\mathbf{x}',t)+\delta R\mathcal{W}_\pm(\mathbf{x}',t)]\,\frac{(\mathbf{x}-\mathbf{x}')\cdot\partial_t\mathbf{x}}{|\mathbf{x}-\mathbf{x}'|^3}\times(1+\varepsilon_{Yukawa}) \\ &= \mathcal{M}^2\Big[\int d^3x'\mathcal{W}_o\frac{\Omega_o r' r_o\sin\theta'\sin(\Omega_o t-\phi')}{[r_o^2+r'^2-2r_o r'\sin\theta'\cos(\Omega_o t-\phi')]^{3/2}} \\ &\quad + \delta R\int d^3x'\mathcal{W}_o\Big\{\frac{F_t(t,r',\theta',\phi')}{[r_o^2+r'^2-2r_o r'\sin\theta'\cos(\Omega_o t-\phi')]^{3/2}} \\ &\qquad - \frac{G_t(t,r',\theta',\phi')}{[r_o^2+r'^2-2r_o r'\sin\theta'\cos(\Omega_o t-\phi')]^{5/2}}\Big\} \\ &\qquad\quad + \delta R\int d^3x'\mathcal{W}_\pm\frac{\Omega_o r' r_o\sin\theta'\sin(\Omega_o t-\phi')}{[r_o^2+r'^2-2r_o r'\sin\theta'\cos(\Omega_o t-\phi')]^{3/2}}\Big] \\ &\qquad\quad \times\left(1+\mathcal{O}\left(\frac{\mathcal{L}}{\lambda_J}\right)\right) \end{aligned} \tag{3.39}$$

where

$$\begin{aligned} F_t(t,r',\theta',\phi') = r'\sin\theta'\Big[\Big(\frac{\Omega_r-2\Omega_o^2}{\Omega_r}\Big)\sin(\Omega_r t)\cos(\Omega_r t-\phi') \\ - \Omega_o\cos(\Omega_r t)\sin(\Omega_o t-\phi')\Big] - \Omega_r r_o\sin(\Omega_r t)\end{aligned} \tag{3.40}$$

$$G_t(t,r',\theta',\phi') = 3\Omega_o r' r_o\sin^2\theta'\sin(\Omega_o t-\phi')X(t,r',\theta',\phi') \tag{3.41}$$

We can observe that for the limit when the perturbation parameter $\delta R = 0$, the expression simplifies to Barausse's result [16] in spherical coordinates.

3.4.2 Metric perturbations in r

The same prescription as that for the metric perturbations in t are presented for r and ϕ. Expressing the projection of the separation vector onto the r derivative of the position vector of the perturber yields,

$$\begin{aligned}(\mathbf{x}-\mathbf{x}')\cdot\partial_r\mathbf{x} &= R(t) - r'\sin(\theta')\cos(\Phi(t)-\phi') \\ &= r_o - r'\sin\theta'\cos(\Omega_o t-\phi') \\ &\quad + \delta R\left[\cos(\Omega_r t) - \frac{2\Omega_o}{\Omega_r}\frac{r'}{r_o}\sin(\Omega_r t)\sin\theta'\sin(\Omega_o t-\phi')\right]\end{aligned} \tag{3.42}$$

Substituting the previous expression to I_r yields,

$$\begin{aligned} I_r = \mathcal{M}^2 \Big[\int d^3x' \mathcal{W}_o & \frac{r_o - r' \sin\theta' \cos(\Omega_o t - \phi')}{[r_o^2 + r'^2 - 2r_o r' \sin\theta' \cos(\Omega_o t - \phi')]^{3/2}} \\ + \delta R \int d^3x' \mathcal{W}_o & \Big\{ \frac{F_r(t, r', \theta', \phi')}{[r_o^2 + r'^2 - 2r_o r' \sin\theta' \cos(\Omega_o t - \phi')]^{3/2}} \\ & - \frac{G_r(t, r', \theta', \phi')}{[r_o^2 + r'^2 - 2r_o r' \sin\theta' \cos(\Omega_o t - \phi')]^{5/2}} \Big\} \\ & + \delta R \int d^3x' \mathcal{W}_\pm \frac{r_o - r' \sin\theta' \cos(\Omega_o t - \phi')}{[r_o^2 + r'^2 - 2r_o r' \sin\theta' \cos(\Omega_o t - \phi')]^{3/2}} \Big] \\ & \times \left(1 + \mathcal{O}\left(\frac{\mathcal{L}}{\lambda_J}\right)\right) \end{aligned} \tag{3.43}$$

where

$$F_r(t, r', \theta', \phi') = \cos(\Omega_r t) - \frac{2\Omega_o}{\Omega_r} \frac{r'}{r_o} \sin(\Omega_r t) \sin\theta' \sin(\Omega_o t - \phi') \tag{3.44}$$

$$G_r(t, r', \theta', \phi') = 3 \sin\theta' (r_o - r' \sin\theta' \cos(\Omega_o t - \phi')) X(t, r', \theta', \phi') \tag{3.45}$$

3.4.3 Metric perturbations in ϕ

Lastly, we deal with the metric perturbations in ϕ in the same way as we did for the previous cases. Expanding the projection of the separation vector onto the angular derivative of the perturber's position vector yields.

$$\begin{aligned} (\mathbf{x} - \mathbf{x}') \cdot \partial_\phi \mathbf{x} = r_o r' \sin\theta' \sin(\Omega_o t - \phi') & \\ + \delta R \Big[r' \sin\theta' \cos(\Omega_r t) \sin(\Omega_o t - \phi') & \\ + 2 \frac{\Omega_o}{\Omega_r} r' \sin\theta' \sin(\Omega_r t) \cos(\Omega_o t - \phi') \Big] & \end{aligned} \tag{3.46}$$

We expand I_ϕ in δR while keeping all terms in linear order and obtain,

$$\begin{aligned} I_\phi = \mathcal{M}^2 \Big[\int d^3x' \mathcal{W}_o & \frac{r_o r' \sin\theta' \sin(\Omega_o t - \phi')}{[r_o^2 + r'^2 - 2r_o r' \sin\theta' \cos(\Omega_o t - \phi')]^{3/2}} \\ + \delta R \int d^3x' \mathcal{W}_o & \Big\{ \frac{F_\phi(t, r', \theta', \phi')}{[r_o^2 + r'^2 - 2r_o r' \sin\theta' \cos(\Omega_o t - \phi')]^{3/2}} \\ & - \frac{G_\phi(t, r', \theta', \phi')}{[r_o^2 + r'^2 - 2r_o r' \sin\theta' \cos(\Omega_o t - \phi')]^{5/2}} \Big\} \\ & + \delta R \int d^3x' \mathcal{W}_\pm \frac{r_o r' \sin\theta' \sin(\Omega_o t - \phi')}{[r_o^2 + r'^2 - 2r_o r' \sin\theta' \cos(\Omega_o t - \phi')]^{3/2}} \Big] \\ & \times \left(1 + \mathcal{O}\left(\frac{\mathcal{L}}{\lambda_J}\right)\right) \end{aligned} \tag{3.47}$$

where

$$
\begin{aligned}
F_\phi(t, r', \theta', \phi') &= r' \sin\theta' \cos(\Omega_r t)\sin(\Omega_o t - \phi') \\
&\qquad + 2\frac{\Omega_o}{\Omega_r} r' \sin\theta' \sin(\Omega_r t)\cos(\Omega_o t - \phi') \qquad (3.48) \\
G_\phi(t, r', \theta', \phi') &= 3 r_o r' \sin^2\theta' \sin(\Omega_o t - \phi') X(t, r', \theta', \phi') \qquad (3.49)
\end{aligned}
$$

3.4.4 Some remarks

The expressions for the metric perturbations that we have derived can be used to compute the perturbed four-acceleration [48] to linear order,

$$
\begin{aligned}
\tilde{a}^\mu_{pert} &= \frac{\mathrm{d}^2 \tilde{x}^\mu_{pert}}{\mathrm{d}\tau^2} \\
&= -\frac{1}{2}(\eta^{\mu\nu} + u^\mu_{pert} u^\nu_{pert})(2\delta g_{\nu\lambda,\rho} - \delta g_{\lambda\rho,\nu}) u^\lambda u^\rho + \mathcal{O}(M^2) \qquad (3.50)
\end{aligned}
$$

Further, by projecting the perturbed four-force $\tilde{F}^\mu_{pert} = M\tilde{a}^\mu_{pert}$ onto a comoving tetrad along the trajectory of the orbit, one can obtain the change in three-momentum of the particle in the rest frame, which corresponds to the dynamical friction experienced by the particle. We leave the evaluation of these terms for future work as it is not within the scope of the study.

Chapter 4

Generalization and future work

We have pursued an analytic approach in studying the density wake induced by a perturber moving along a slightly-eccentric orbit immersed in a tenuous fluid in flat spacetime. This work is a precursor to the slightly-eccentric extension of the study of relativistic dynamical friction effects by Barausse. The density perturbation induced by a slightly-eccentric orbit appears to deviate from its circular orbit counterpart only in the transonic case ($\mathcal{M} \sim 0.8 - 1.3$), where equally spaced density trails manifest, but decreases in magnitude as we consider points farther from the perturber. This can be attributed to the perturbation (perihelion frequency, Ω_r) introduced on the radial component of the orbit. However, this effect is not observed for both subsonic ($\mathcal{M} < 0.8$) and supersonic ($\mathcal{M} \sim 1.3 - 5.0$) cases.

Extending our formulation to the eccentric case will shed more light on the possible effect of gaseous environments on the evolution of EMRIs. Further, by considering a spacetime with a central singularity (e.g. Schwarzschild, Kerr), like in Ref [42], for the same slightly-eccentric formulation, we can resolve the previously discussed inconsistency of the flat spacetime approximation that we have applied. In this study, we have only considered a static fluid of constant energy density and pressure in all space. Using a more realistic case, such as EMRIs surrounded by a rotating accretion disk, can be an interesting case to look at in the future. One can also use a post-Newtonian metric instead of just flat spacetime. Also, introducing a uniform large-scale magnetic field into the spacetime can bring about interesting physics, as in Ref [54].

This attempt to extend the formulation of dynamical friction to the eccentric case also has an important role in probing the environment of EMRIs in highly dense environments. Coupling this extension to a nonlinear perturbation analysis can give us a model for the evolution of very massive double perturbers (ie. merger of an intermediate-mass black hole and a supermassive black hole) in gaseous environments which was done in the Newtonian formulation by Refs [49, 53].

Appendix A

Weight function, $\mathcal{W}(x', t)$

We were able to analytically solve for the density perturbation over all space by employing a spherical decomposition on the source, and a separation of variables for the wave equation. The form of the solution inside and outside the orbital radius r_o is given by,

$$\frac{\delta n}{n}(\mathbf{x}, t) = \sum_{\omega} \sum_{lm} \Psi^{\omega}_{lm} e^{-i\omega t} Y_{lm}(\theta, \phi) \tag{A.1}$$

where $\omega = \{\omega^o_m, \omega^{\pm}_m\}$ and $l = 0, ..., n, m = -l, ..., l$.

In order to follow the analysis by Barausse [16], we manipulate the expression that we were able to obtain by factoring out some constant terms, and finally derive a weight function $\mathcal{W}(x', t)$ that is faithful to the prescription by Ref [16] and [14].

A.1 Solution inside the orbital radius

The solution inside the orbital radius has the form,

$$\begin{aligned}\Psi_{in}(\mathbf{x}, t) = &\sum_{l,m \neq o} A_{lm} j_l \left(\frac{\omega^o_m}{c_s} r \right) e^{-i\omega^o_m t} Y_{lm}(\theta, \phi) \\ &+ \sum_{l,m} A^+_{lm} j_l \left(\frac{\omega^+_m}{c_s} r \right) e^{-i\omega^+_m t} Y_{lm}(\theta, \phi) \\ &+ \sum_{l,m} A^-_{lm} j_l \left(\frac{\omega^-_m}{c_s} r \right) e^{-i\omega^-_m t} Y_{lm}(\theta, \phi) \\ &+ \sum_{l} A_l r^l Y_{l0}(\theta, \phi) + B_{00} Y_{00}(\theta, \phi)\end{aligned} \tag{A.2}$$

where the coefficients are given in Chapter 3. We massage these coefficients for us to obtain the following

$$\begin{aligned} A_{lm} &= -\Gamma \frac{c_s^2 Y^*_{lm}\left(\frac{\pi}{2},0\right)}{f^o_{lm}} \\ &= -\Gamma \Lambda_{lm} \end{aligned} \tag{A.3}$$

$$\begin{aligned} A^{\pm}_{lm} &= -\Gamma Y^*_{lm}\left(\frac{\pi}{2},0\right) f^{\pm}_{lm}(r_o) \\ &= -\Gamma \Lambda^{\pm}_{lm} \end{aligned} \tag{A.4}$$

$$\begin{aligned} A_l &= \Gamma \frac{Y^*_{l0}\left(\frac{\pi}{2},0\right)}{(2l+1)r_o^l} \\ &= \Gamma \Lambda_l \end{aligned} \tag{A.5}$$

$$\begin{aligned} B_{00} &= -\Gamma Y^*_{00}\left(\frac{\pi}{2},0\right) \\ &= \Gamma \beta_{00} \end{aligned} \tag{A.6}$$

where

$$\Gamma = \frac{2\pi M \gamma \left(1+v^2\right)}{c_s^2}.$$

This gives us our solution in terms of the weight function $\mathcal{W}(\mathbf{x},t)$,

$$\Psi_{in}(\mathbf{x},t) = \Gamma \mathcal{W}_{in}(\mathbf{x},t)$$

A.2 Solution outside the orbital radius

Outside the orbital radius, the solution for the density perturbation is given by

$$\begin{aligned} \Psi_{out}(\mathbf{x},t) = \sum_{l,m\neq o} & C_{lm} h_l^{(1)}\left(\frac{\omega^o_m}{c_s} r\right) e^{-i\omega^o_m t} Y_{lm}(\theta,\phi) \\ & + \sum_{l,m} C^+_{lm} h_l^{(1)}\left(\frac{\omega^+_m}{c_s} r\right) e^{-i\omega^+_m t} Y_{lm}(\theta,\phi) \\ & + \sum_{l,m} C^-_{lm} h_l^{(1)}\left(\frac{\omega^-_m}{c_s} r\right) e^{-i\omega^-_m t} Y_{lm}(\theta,\phi) \\ & + \sum_{l} A_l r^{-1(l+1)} Y_{l0}(\theta,\phi) - \frac{C_{00}}{r} Y_{00}(\theta,\phi) \end{aligned} \tag{A.7}$$

which, in the same manner, we recast into the following form,

$$\begin{aligned}
C_{lm} &= A_{lm}\frac{j_l\left(\frac{\omega_m^o}{c_s}r\right)}{h_l^{(1)}\left(\frac{\omega_m^o}{c_s}r\right)} \\
&= -\Gamma\Lambda_{lm}\frac{j_l\left(\frac{\omega_m^o}{c_s}r\right)}{h_l^{(1)}\left(\frac{\omega_m^o}{c_s}r\right)} \qquad \text{(A.8)} \\
C_{lm}^{\pm} &= A_{lm}^{\pm}\frac{j_l\left(\frac{\omega_m^{\pm}}{c_s}r\right)}{h_l^{(1)}\left(\frac{\omega_m^{\pm}}{c_s}r\right)} \\
&= -\Gamma\Lambda_{lm}^{\pm}\frac{j_l\left(\frac{\omega_m^{\pm}}{c_s}r\right)}{h_l^{(1)}\left(\frac{\omega_m^{\pm}}{c_s}r\right)} \qquad \text{(A.9)} \\
D_l &= A_l r_o^{(2l+1)} = \Gamma\Lambda_l \qquad \text{(A.10)} \\
C_{00} &= -B_{00}r_o = -\Gamma\beta_{00}r_o \qquad \text{(A.11)}
\end{aligned}$$

where

$$\Gamma = \frac{4\pi M\gamma\left(1+v^2\right)r_o}{c_s^2}.$$

and give us the solution outside the orbital radius in terms of the weight function $\mathcal{W}_{out}$,

$$\Psi_{out}(\mathbf{x},t) = \Gamma\mathcal{W}_{out}(\mathbf{x},t)$$

Bibliography

[1] S Chandrasekhar. I. General Considerations: The Coefficient of Dynamical Friction. *Astrophys J*, 97:255–262, 1943.

[2] Tj R Bontekoe and TS van Albada. Decay of galaxy satellite orbits by dynamical friction. *Mon Not Roy Astron Soc*, 224:349–366, 1987.

[3] S Cora, J Muzzio, and M Marcela Vergne. Orbital decay of galactic satellites as a result of dynamical friction. *Mon Not Roy Astron Soc*, 289(2):253–262, 1997.

[4] M Fujii, Y Funato, and J Makino. Dynamical friction on satellite galaxies. *Publ Astron Soc Jpn*, 58(4):743–752, 2006.

[5] Nader Haghighipour. Dynamical friction and resonance trapping in planetary systems. *Mon Not Roy Astron Soc*, 304(1):185–194, 1999.

[6] E Grishin and HB Perets. Application of Gas Dynamical Friction for Planetesimals. I. Evolution of Single Planetesimals. *Astrophys J*, 811(1):54, 2015.

[7] S Kim and M Morris. Dynamical Friction on Star Clusters near the Galactic Center. *Astrophys J*, 597:312–322, 2003.

[8] M Fujii, M Iwasawa, Y Funato, and J Makino. Evolution of Star Clusters near the Galactic Center: Fully SelfConsistent N Body Simulations. *Astrophys J*, 686(2):1082–1093, 2008.

[9] A Petts and A Gualandris. Infalling Young Clusters in the Galactic Centre : implications for IMBHs and young stellar populations. *Mon Not Roy Astron Soc*, 467:3775–3787, 2017.

[10] E Lee. Dynamical friction in the post-Newtonian approximation of general relativity. *Astrophys J*, 155(February):687–696, 1969.

[11] L Petrich, S Shapiro, R Stark, and S Teukolsky. Accretion onto a moving black hole: a fully relativistic treatment. *Astrophys J*, 336:313–349, 1989.

[12] Y Rephaeli and EE Salpeter. Flow past a massive object and the gravitational drag. *Astrophys J*, 240:20–24, 1980.

[13] EC Ostriker. Dynamical Friction in a Gaseous Medium. *Astrophys J*, 513(1):252–258, 1999.

[14] H Kim and WT Kim. Dynamical Friction of a Circular-orbit perturber in a gaseous medium. *Astrophys J*, 665(2007):432–444, 2007.

[15] P Amaro-Seoane, JR Gair, A Pound, SA Hughes, and CF Sopuerta. Research Update on Extreme-Mass-Ratio Inspirals. *J Phys Conf Ser*, 610(1), 2015.

[16] E Barausse. Relativistic dynamical friction in a collisional fluid. *Mon Not Roy Astron Soc*, 382(2):826–834, 2007.

[17] J Binney and S Tremaine. Dynamical Friction. In *Galactic dynamics*, chapter Chapter 7, pages 417–488. Princeton University Press, New Jersey, 1987.

[18] GE Uhlenbeck and LS Ornstein. On the theory of the Brownian motion. *Phys Rev D*, 36(5):823–841, 1930.

[19] M Falco, SH Hansen, R Wojtak, and GA Mamon. Why does the jeans swindle work? *Mon Not Roy Astron Soc L*, 431(1):6–9, 2013.

[20] D Arovas. Lecture notes on thermodynamics and statistical mechanics, 2013.

[21] A A Vlasov. The vibrational properties of an electron gas. *Soviet Physics Uspekhi*, 10(6):721, 1968.

[22] J Binney and S Tremaine. Equilibria of Collisionless Systems. In *Galactic dynamics*, chapter Chapter 4, pages 190–195. Princeton University Press, New Jersey, 1987.

[23] VP Dokuchaev. Emission of magnetoacoustic waves in the motion of stars in cosmic space. *Sov Astron*, 8(1):23–31, 1964.

[24] MA Ruderman and EA Spiegel. Galactic Wakes. *Astrophys J*, 165:1–15, 1971.

[25] L Miller. Heating and cooling in clusters of galaxies. *Mon Not Roy Astron Soc*, 220:713–722, 1986.

[26] FD Ryan. Gravitational waves from the inspiral of a compact object into a massive, axisymmetric body with arbitrary multipole moments. *Phys Rev D*, 52(10):5707–5718, 1995.

[27] B.P Abbott and Others. Observation of gravitational waves from a binary black hole merger. *Phys Rev Lett*, 116(6):1–16, 2016.

[28] JR Gair, S Babak, A Sesana, P Amaro-Seoane, E Barausse, CPL Berry, E Berti, and C Sopuerta. Prospects for observing extreme-mass-ratio inspirals with LISA. *J Phys Conf Ser*, 840(1), 2017.

[29] DF Figer. Massive Star Formation in the Galactic Center. *Proceedings of the International Astronomical Union*, 250:247–256, 2008.

[30] R Blandford and M Begelman. On the Fate of Gas Accreting at a Low Rate onto a Black Hole. *Mon Not Roy Astron Soc*, 303(1):L1–L5, 1999.

[31] O Zanotti, J Font, L Rezzolla, and P Montero. Dynamics of oscillating relativistic tori around Kerr black holes. *Mon Not Roy Astron Soc*, 356(January):1371–1382, 2005.

[32] R Narayan. Hydrodynamic Drag on a Compact Star Orbiting a Supermassive Black Hole. *Astrophys J*, 536(2):663–667, 2000.

[33] JH Krolik. *Active Galactic Nuclei: From the Central Black Hole to the Galactic Environment.* Princeton University Press, New Jersey, 1999.

[34] J Huchra and R Burg. The spatial distribution of active galactic nuclei I. The Density of Seyfert Galaxies and Liners. *Astrophys J*, 393:90–97, 1992.

[35] T Di Matteo, AC Fabian, CL Carilli, and RJ Ivison. Testing the ADAF Paradigm for supermassive black holes in elliptical galaxies. *Adv Space Res*, 23(516):1075–1078, 1999.

[36] T Di Matteo, CL Carilli, and AC Fabian. Limits on the Accretion Rates onto Massive Black Holes in Nearby Galaxies. *Astrophys J*, 547:731–739, 2001.

[37] R Narayan, I Yi, and R Mahadevan. Explaining the spectrum of Sagittarius A* with a model of an accreting black hole. *Nature*, 374(6523):623–625, 1995.

[38] X Chen, MA Abramowicz, JP Lasota, R Narayan, and I Yi. Unified description of accretion flows around black holes. *Astrophys J*, 443:L61–L64, 1995.

[39] D Vokroulicky and V Karas. A star orbiting around a supermassive rotating black hole: free motion and corrections due to star-disc collisions. *Mon Not Roy Astron Soc*, 265:365–378, 1993.

[40] L Subr and V Karas. An orbiter crossing an accretion disc. *Astronomy and Astrophysics*, 352:452–458, 1999.

[41] V Karas and L Subr. Orbital decay of satellites crossing an accretion disc. *Astronomy and Astrophysics*, 696:686–696, 2001.

[42] E Barausse and L Rezzolla. Influence of the hydrodynamic drag from an accretion torus on extreme mass-ratio inspirals. *Phys Rev D*, 77(10):1–22, 2008.

[43] P Amaro-Seoane, JR Gair, M Freitag, MC Miller, I Mandel, CJ Cutler, and S Babak. Intermediate and extreme mass-ratio inspirals - Astrophysics, science applications and detection using LISA. *Classical Quant Grav*, 24(17):R113–R169, 2007.

[44] LM Diaz-Rivera, E Messaritaki, B Whiting, and S Detweiler. Scalar field self-force effects on orbits about a Schwarzschild black hole. *Phys Rev D*, 70(12):14, 2004.

[45] T Apostolatos, D Kennefick, A Ori, and E Poisson. Gravitational radiation from a particle in circular orbit around a black hole. III. Stability of circular orbits under radiation reaction. *Phys Rev D*, 47(12):5376–5388, 1993.

[46] H Kodama and M Sasaki. Cosmological Perturbation Theory. *Prog Theor Phys*, (78), 1984.

[47] CP Ma and E Bertschinger. Cosmological perturbation theory in the synchronous and conformal Newtonian gauges. *Astrophys J*, 455:7–25, 1995.

[48] E Poisson, A Pound, and I Vega. The motion of point particles in curved spacetime. *Living Rev Relativ*, 14:1–162, 2011.

[49] H Kim and WT Kim. Nonlinear dynamical friction in a gaseous medium. *Astrophys J*, 703(2):1278–1293, 2009.

[50] L Blanchet, A Spallicci, and B Whiting, editors. *Mass and Motion in General Relativity.* Springer Science & Business Media, illustrate edition, 2011.

[51] A Escala, RB Larson, PS Coppi, and D Mardones. The role of gas in the merging of massive black holes in galactic nuclei. I. Black hole merging in a spherical gas cloud. *Astrophys J*, 607(1):765–777, 2004.

[52] M Dotti, M Colpi, and F Haardt. Laser Interferometer Space Antenna double black holes: Dynamics in gaseous nuclear discs. *Mon Not Roy Astron Soc*, 367(1):103–112, 2006.

[53] H Kim, WT Kim, and FJ Sanchez-Salcedo. Dynamical Friction of Double Perturbers in a Gaseous Medium. *Astrophys J*, 679(May):L33–L36, 2008.

[54] FJ Sánchez-Salcedo. Dynamical friction in a gaseous medium with a large-scale magnetic field. *Astrophys J*, 745(2), 2012.